frontiers | Frontiers in Marine Science

TYPE Original Research
PUBLISHED 08 December 2022
DOI 10.3389/fmars.2022.902062

OPEN ACCESS

EDITED BY
Annie Bourbonnais,
University of South Carolina,
United States

REVIEWED BY
Karen L. Casciotti,
Stanford University, United States
Xin Zhou,
Guangdong Ocean University, China
Su Mei Liu,
Ocean University of China, China

*CORRESPONDENCE
Andrew W. Dale
adale@geomar.de

†PRESENT ADDRESS
Frederike Korth,
Institute of Agricultural Engineering,
University of Natural Resources and
Life Sciences, Wien, Austria

SPECIALTY SECTION
This article was submitted to
Marine Biogeochemistry,
a section of the journal
Frontiers in Marine Science

RECEIVED 22 March 2022
ACCEPTED 10 November 2022
PUBLISHED 08 December 2022

CITATION
Dale AW, Clemens D, Dähnke K,
Korth F, Wankel SD,
Schroller-Lomnitz U, Wallmann K and
Sommer S (2022) Nitrogen cycling in
sediments on the NW African margin
inferred from N and O isotopes in
benthic chambers.
Front. Mar. Sci. 9:902062.
doi: 10.3389/fmars.2022.902062

Nitrogen cycling in sediments on the NW African margin inferred from N and O isotopes in benthic chambers

Andrew W. Dale[1]*, David Clemens[1], Kirstin Dähnke[2], Frederike Korth[1†], Scott D. Wankel[3], Ulrike Schroller-Lomnitz[1], Klaus Wallmann[1] and Stefan Sommer[1]

[1]GEOMAR Helmholtz Centre for Ocean Research Kiel, Kiel, Germany, [2]Institute of Carbon Cycles, Helmholtz Centre Hereon, Geesthacht, Germany, [3]Department of Marine Chemistry and Geochemistry, Woods Hole Oceanographic Institution, Woods Hole, MA, United States

Benthic nitrogen cycling in the Mauritanian upwelling region (NW Africa) was studied in June 2014 from the shelf to the upper slope where minimum bottom water O_2 concentrations of 25 µM were recorded. Benthic incubation chambers were deployed at 9 stations to measure fluxes of O_2, dissolved inorganic carbon (DIC) and nutrients (NO_3^-, NO_2^-, NH_4^+, PO_4^{3-}, H_4SiO_4) along with the N and O isotopic composition of nitrate ($\delta^{15}N\text{-}NO_3^-$ and $\delta^{18}O\text{-}NO_3^-$) and ammonium ($\delta^{15}N\text{-}NH_4^+$). O_2 and DIC fluxes were similar to those measured during a previous campaign in 2011 whereas NH_4^+ and PO_4^{3-} fluxes on the shelf were 2 – 3 times higher and possibly linked to a long-term decline in bottom water O_2 concentrations. The mean isotopic fractionation of NO_3^- uptake on the margin, inferred from the loss of NO_3^- inside the chambers, was 1.5 ± 0.4 ‰ for $^{15/14}N$ ($^{15}\epsilon_{app}$) and 2.0 ± 0.5 ‰ for $^{18/16}O$ ($^{18}\epsilon_{app}$). The mean $^{18}\epsilon_{app}$:$^{15}\epsilon_{app}$ ratio on the shelf (< 100 m) was 2.1 ± 0.3, and higher than the value of 1 expected for microbial NO_3^-reduction. The $^{15}\epsilon_{app}$ are similar to previously reported isotope effects for NO_3^- respiration in marine sediments but lower than determined in 2011 at a same site on the shelf. The sediments were also a source of ^{15}N-enriched NH_4^+ (9.0 ± 0.7 ‰). A numerical model tuned to the benthic flux data and that specifically accounts for the efflux of ^{15}N-enriched NH_4^+ from the seafloor, predicted a net benthic isotope effect of N loss ($^{15}\epsilon_{sed}$) of 3.6 ‰; far above the more widely considered value of ~0‰. This result is further evidence that the assumption of a universally low or negligible benthic N isotope effect is not applicable to oxygen-deficient settings. The model further suggests that $^{18}\epsilon_{app}$:$^{15}\epsilon_{app}$ trajectories > 1 in the benthic chambers are most likely due to aerobic ammonium oxidation and nitrite oxidation in surface sediments rather than anammox, in agreement with published observations in the water column of oxygen deficient regions.

KEYWORDS

nitrogen isotopes, fractionation, particulate organic carbon (POC), continental margin, denitrification, anammox, NW Africa upwelling, marine sediments

1 Introduction

The Canary upwelling region along the north-western African coast is an important eastern boundary current system with regard to primary production (0.33 Gtons C yr^{-1}), second in magnitude only to the Benguela upwelling (Carr, 2001). Off Mauritania, high primary production is driven by upwelling of nutrient-rich South Atlantic Central Water (SACW) and huge dust inputs from the adjacent Sahara-Sahel region (Fischer et al., 2010). Subsurface waters off Mauritania are better ventilated than the Benguela system and the other large upwelling systems in the Eastern Tropical Pacific, with minimum bottom water dissolved O_2 levels on the margin of several tens of micromoles per liter (Hartmann et al., 1976; Dale et al., 2014; Thomsen et al., 2019). However, the SACW in the Eastern Tropical North Atlantic (ETNA) appears to be undergoing significant deoxygenation of ca. 0.5 µmol kg^{-1} yr^{-1} (Stramma et al., 2008), possibly due to a warming-induced decrease in solubility and biological O_2 consumption (Schmidtko et al., 2017). At this rate, subsurface waters on the Mauritanian margin are heading towards anoxia by the end of the 21st century.

In the Eastern Tropical Pacific and South Atlantic upwelling systems, the anoxic water column is a hotspot of microbially-mediated N loss, either by denitrification (nitrate reduction to N_2) and/or anammox (anaerobic oxidation of ammonium by nitrite to N_2) (Devol et al., 2006; Lam and Kuypers, 2011). Along with the Arabian Sea and Bay of Bengal, most fixed N loss in ocean waters occurs in these 'oxygen minimum zones (OMZ)' (Gruber, 2008). In sediments, by contrast, and with the possible exception of the oligotrophic deep-sea and euxinic basins, microbial transformation of fixed N to N_2 by microorganisms occurs almost everywhere (Middelburg et al., 1996). In the Mauritanian OMZ, where pelagic O_2 concentrations are consistently above the inhibition threshold for denitrification (ca. 5 µM), benthic denitrification/anammox is the only significant N loss pathway. Benthic denitrification rates measured using ^{15}N-labelling techniques range from around 4 mmol N m^{-2} d^{-1} on the shelf to 1 mmol N m^{-2} d^{-1} on the upper slope (Sokoll et al., 2016), and are toward the higher end for open-ocean continental margins. Anammox was found to be of minor importance (Sokoll et al., 2016).

Current understanding of the fixed N balance in the ocean is dependent on knowledge of the rates of N transformation pathways, both in the water column and in the sediment. To a large extent, this is achieved by balancing the marine inventory of stable N isotopes (^{14}N and ^{15}N) under steady state conditions (Brandes and Devol, 2002). This approach is possible because most microbial N transformation processes impart unique degrees of isotopic discrimination, or fractionation, of one isotope over another, expressed as a kinetic isotope effect (KIE), or ϵ (unit: ‰). (In this paper, $\epsilon = (\alpha - 1)\cdot 1000$, where α is the fractionation factor defined as ${}^{L}k/{}^{H}k$, and where k denotes the reaction rate constant of the heavy (H) and light (L) isotopologues). Studies in the water column and in the laboratory have revealed a wealth of information concerning N and O effects of microbial N cycling (e.g. Sigman et al., 2006; Casciotti and McIlvin, 2007; Granger et al., 2008; Buchwald and Casciotti, 2013; Gaye et al., 2013; Bourbonnais et al., 2015 and many others). For instance, the N and O isotope effects during the dissimilatory reduction of nitrate (NO_3^-) to nitrite (NO_2^-) are similar at ca. 15 – 30 ‰ in favor of the lighter isotopes (Voss et al., 2001; Kritee et al., 2012; Bourbonnais et al., 2015). Oxidation of NO_2^- to NO_3^-, in contrast, has an inverse isotope effect due to fractionation at the enzymatic level during N–O bond formation by nitrite oxidoreductase (Casciotti, 2009). NO_2^- oxidation leads to enrichment of ^{14}N and ^{16}O in the residual NO_2^- and an enrichment of ^{15}N and ^{18}O in the NO_3^- product (Casciotti, 2009). This divergence has led numerous investigators to conclude that a significant fraction of NO_2^- produced by reduction of NO_3^- in oxygen deficient waters is reoxidized to NO_3^- (Casciotti and McIlvin, 2007; Buchwald and Casciotti, 2013; Casciotti et al., 2013; Gaye et al., 2013; Bourbonnais et al., 2015; Casciotti, 2016; Granger and Wankel, 2016). Fewer studies have been carried out in sediments, although so far it appears that the microbial isotope effects observed in the water column are largely transferrable to the benthic environment (Lehmann et al., 2004; Lehmann et al., 2007; Alkhatib et al., 2012; Dale et al., 2014; Dale et al., 2019). The major difference between the water column and sediment rests with the much lower isotopic fractionation of NO_3^- uptake by sediments (hereafter benthic fractionation), arising from transport limitation of NO_3^- diffusion within the sediment (< 3 ‰; Brandes and Devol, 1997; Lehmann et al., 2004). Based on this assumption, it is understood that around two-thirds of the global oceanic fixed N loss takes place in the sediment and one-third in OMZ waters (Brandes and Devol, 2002; Somes et al., 2013). However, more recent studies suggest that the benthic N isotope effect may be higher, especially in sediments underlying oxygen-deficient bottom waters (Lehmann et al., 2007; Alkhatib et al., 2012; Dähnke and Thamdrup, 2013; Dale et al., 2014; Dale et al., 2019). Furthermore, it can be enhanced by the efflux of ^{15}N-enriched NH_4^+ from the sediment (Lehmann et al., 2007; Granger et al., 2011; Alkhatib et al., 2012). Accurate estimates of the total benthic N isotope effect that also includes NH_4^+ and other N species, and thus more relevant for the global N budget, require a deeper understanding of the rate of benthic N loss and associated N isotope transformations.

In this study, we deployed *in situ* benthic incubation chambers on the Mauritanian margin in 2014 during the transition from the strong to weak upwelling season (Thomsen et al., 2019). Fieldwork was conducted along a transect from the shallow shelf to the upper slope at 18 °N. Our objective was to determine the recycling rates and exchange fluxes of dissolved inorganic nitrogen (DIN: NO_3^-, NO_2^-, NH_4^+) between the sediment and water column and compare them to results from

an earlier campaign in 2011. We also measured the N and O isotopic composition of NO_3^- (δ^{15}N-NO_3^- and δ^{18}O-NO_3^-) and NH_4^+ (δ^{15}N-NH_4^+) inside the chambers. With this information, and with the help of a numerical model, we were able to calculate the total the benthic N isotope effect along with further information on benthic N turnover rates, sources and transformations.

2 Oceanographic setting

The study area lies within the Mauritanian upwelling region in the ETNA. The prominent water mass that upwells onto the margin at 18 °N is poleward-flowing and nutrient-rich SACW. Upwelling is strongest between January and April when the Intertropical Convergence Zone (ITCZ) migrates southwards (Mittelstaedt, 1983). It weakens when the ITZC moves northwards, leading to a decline in primary production on the shelf. Primary production nonetheless remains relatively high year-round at 80 – 200 mmol m^{-2} d^{-1} of C (Huntsman and Barber, 1977). Oceanographic data indicate that upwelling was active during the fieldwork (Thomsen et al., 2019). Dissolved O_2 levels below the surface mixed layer are dictated by SACW ventilation, vertical mixing, and respiration rates of organic carbon in the water column (Mittelstaedt, 1983; Schafstall et al., 2010; Thomsen et al., 2019). They present a deep minimum of 40 – 50 µM at 400 – 500 m water depth and a shallow minimum of 30 – 50 µM on the shelf at 50 - 100 m (Karstensen et al., 2008; Schroller-Lomnitz et al., 2019; Thomsen et al., 2019). The lowest O_2 levels on the shelf are usually encountered during upwelling relaxation in July and August due to combined effects of stratification and benthic respiration (Klenz et al., 2018). A detailed oceanographic overview of the study area during the fieldwork is described by Thomsen et al. (2019) and water column O_2 measurements at the sampling stations are presented by Schroller-Lomnitz et al. (2019).

The sediments on the margin at 18°N are classified as slightly sandy mud or muddy sand (Dale et al., 2014). They comprise 10 - 20% carbonates with organic C increasing from ~1% on the shelf to 3% at 1000 m water depth (Hartmann et al., 1976; Gier et al., 2017). Sediment reworking by turbulent mixing exports fine-grained particles down the slope (Fütterer, 1983; Schafstall et al., 2010). Consequently, sedimentation rates on the shelf determined by ^{210}Pb accumulation are low, and increase to 350 cm kyr^{-1} below the shelf break (Dale et al., 2014). Porewaters in the upper 20 cm are mostly ferruginous, becoming sulfidic on the shallow shelf (Dale et al., 2014; Gier et al., 2017; Schroller-Lomnitz et al., 2019). Benthic respiration rates on the shelf range from approximately 10 to 20 mmol m^{-2} d^{-1} of C (Dale et al., 2014; Schroller-Lomnitz et al., 2019). These values are typical for the average margin, but far smaller than those in the carbon-rich shelf sediments in the Peruvian and Benguelan upwelling systems (Brüchert et al., 2003; Dale et al., 2015).

3 Material and methods

Data presented here were mostly measured within the framework of the project "Climate – Biogeochemistry Interactions in the Tropical Ocean" (www.sfb754.de) on research campaign M107 (RV Meteor) from 30 May to 3 July 2014. A complete overview of sediment operations can be found in the cruise report (Sommer et al., 2015). Digital links to the data and a general overview of the project are provided by Krahmann et al. (2021).

3.1 Benthic flux measurements

In situ fluxes of O_2, dissolved inorganic carbon (DIC), NO_3^-, NO_2^-, NH_4^+, silicic acid (H_4SiO_4) and N/O isotopes of N species were measured in benthic chambers along an E-W transect at 18.1° N using autonomous Biogeochemical Observatories (BIGO; Sommer et al., 2008). A total of nine BIGO deployments were made at nine stations along a latitudinal transect across the shelf/slope covering a horizontal distance of 50 km from ~50 to ~1110 m water depth (Figure 1). Seven of the stations were revisited from an earlier cruise during March/April 2011, which coincided with the transition between the strong upwelling and weak upwelling seasons (Dale et al., 2014). Geographical coordinates for each station are listed in Schroller-Lomnitz et al. (2019). These workers reported mean PO_4^{3-} and DIC fluxes at each site for the same lander deployments.

The design and implementation of the BIGO landers has been discussed in detail previously (Krahmann et al., 2021). Each BIGO (I and II) contained two circular flux chambers (C1 and C2) with an internal diameter of 28.8 cm where the sediment was incubated for ~30 h. Discrete samples were taken using glass syringes (eight per chamber) at pre-programmed time intervals for chemical analysis. After BIGO recovery, the syringes were immediately transferred to the onboard cool room (4°C) for filtering (0.2 µm) and sub-sampling. Another six water samples were taken from inside each benthic chamber into quartz tubes for analysis of DIC.

Solute fluxes were calculated from the slope of the linear regression of the concentration data versus sampling time and the height of the water inside each chamber. Fluxes represent the net flux by diffusion/advection in addition to solute pumping by animals (bioirrigation). A total of 29 nutrient data points from the whole data set (n = 720) set were visually assigned as outliers and omitted from the calculations. Twelve DIC data were removed from 90 data points, mainly corresponding to the last syringe samples taken from the chambers on the shelf. For the calculation of the O_2 flux, equal to total oxygen uptake (TOU), the linear initial part of the O_2 time series recorded by optodes (see below) was used. Negative fluxes denote net uptake by the sediment and positive fluxes net release.

3.2 Sediment sampling

Sediment cores at each station were retrieved using a multiple-corer (MUC). Porewaters and particulates were extracted from the sediment as described by Schroller-Lomnitz et al. (2019) and Gier et al. (2017). Further details are provided in those publications.

3.3 Analytical methods

Nutrients in the benthic landers were analyzed on board with a Quaatro Autoanalyzer (Seal Analytic) using standard photometric approaches. Porewaters were analyzed for ferrous iron (Fe^{2+}), NO_3^-, NO_2^-, NH_4^+, PO_4^{3-}, H_4SiO_4, total alkalinity (TA) and hydrogen sulfide (H_2S). Analytical details can be found in Gier et al. (2017); Schroller-Lomnitz et al. (2019) and Sommer et al. (2015). Sediment samples were also stored refrigerated for analysis of solid phase constituents and physical properties at the home laboratory.

The O_2 concentration and temperature inside each chamber were measured using optodes. Bottom water O_2 values were taken from additional optodes mounted externally on the landers. DIC measurements were performed using a quadrupole membrane inlet mass spectrometer (MIMS, GAM200, In Process Instruments) following Sommer et al. (2015). The instrument was equipped with inline sample acidification to convert DIC to dissolved CO_2 gas for measurement at a mass-to-charge ratio of 44.

The particulate organic carbon (POC) content of freeze-dried and milled sediment samples was determined by flash combustion in a Carlo Erba Elemental Analyzer (NA 1500) with an analytical precision and detection limit of 0.04% (dry weight percent) and 0.05%, respectively. POC contents have been published previously (Schroller-Lomnitz et al., 2019). Samples were decarbonated with 0.25 N HCl prior to analysis. Carbonate (assumed to be $CaCO_3$) was determined by weight difference. The precision and detection limit of the carbonate analysis was 2% and 0.1%, respectively. Total particulate nitrogen was determined on the elemental analyzer with the same precision and detection limit as carbonate. We assumed that this is equal to particulate organic N (PON). Porosity was determined from the weight difference of the wet and freeze–dried sediment, assuming a sediment density of 2.5 g cm^{-3} and a seawater density of 1.023 g cm^{-3}.

During a separate field campaign in July 2019 (M156, Sommer et al., 2020), surface sediment close to St. 5 (182 m depth) was analyzed for $\delta^{15}N$ and $\delta^{13}C$ using a high sensitivity elemental analyzer (HSEA) connected to an isotope ratio mass spectrometer (DeltaPlus Advantage, Thermo Fisher Scientific) as described by Hansen and Sommer (2007). $\delta^{15}N$ and $\delta^{13}C$ values of the bulk particulate material (after removing carbonates) were calculated as:

$$\delta^{H}X = \left(\frac{\left({}^{H}X/{}^{L}X\right)_{Sample}}{\left({}^{H}X/{}^{L}X\right)_{Standard}} - 1 \right) \cdot 1000 \quad (1)$$

where $\delta^{H}X$ denotes the isotopic composition (‰) of X (C or N) and H and L are the heavy and light isotopologue of C (13) or N (15). The reference standards were V-PDB for C and N_2 in air for N. System calibration was implemented by the combustion of International Atomic Energy Agency (IAEA-N-1, IAEA-N-2, IAEA-NO-3) and National Institute of Standards and Technology (NBS-22 and NBS-600) compounds. Acetanilide was used as an internal standard after every sixth sample within each sample run. The overall standard deviation (SD) for the low measurement range 2.5 - 8 µg N and 5.0 - 80 µg C was ± 0.25 ‰ and ± 0.2 ‰, respectively. The overall SD for the higher measurement range 3 - 15 µg N and 10 - 140 µg C was ± 0.2 ‰ and ± 0.15‰, respectively.

Benthic lander samples were analyzed for the isotopic composition of nitrate ($\delta^{15}N\text{-}NO_3^-$ and $\delta^{18}O\text{-}NO_3^-$) and ammonium ($\delta^{15}N\text{-}NH_4^+$). Most of the samples were analyzed for $\delta^{15}N\text{-}NO_3^-$ and $\delta^{18}O\text{-}NO_3^-$ at GEOMAR (Kiel, Germany). At three stations (St. 1, 2 and 4), $\delta^{15}N\text{-}NO_3^-$ and $\delta^{18}O\text{-}NO_3^-$ were measured at the Helmholtz Center Hereon (Geesthacht, Germany). In both labs, nitrate dual isotopes were analyzed using the denitrifier method (Sigman et al., 2001; Casciotti et al., 2002). All samples for $\delta^{15}N\text{-}NH_4^+$ were analyzed at GEOMAR using the hypobromite/azide-method (Mcilvin and Altabet, 2005; Zhang et al., 2007). $\delta^{15}N\text{-}NH_4^+$ was only measured in benthic lander samples on the shelf where NH_4^+ concentrations were above the detection limit for a reliable isotope analysis (1 µM). Due to limited sample availability and low NO_2^- concentrations, $\delta^{15}N\text{-}NO_2^-$ could not be measured.

The denitrifier method and the hypobromite/azide-method are based on the isotopic analysis of nitrous oxide (N_2O). In the denitrifier method, NO_3^- and NO_2^- are quantitatively converted to N_2O by *Pseudomonas aureofaciens* (ATTC 13985). The hypobromite/azide-method is based on the chemical conversion of NH_4^+ to N_2O by a subsequent addition of a hypobromite and azide solution. For both methods, the sample volume was adjusted to a sample size of 10 nmol of N_2O. N_2O was extracted from the sample vials by purging with helium and measured with a GasBench II, coupled to an isotope ratio mass spectrometer (Delta Plus, Thermo Fisher Scientific, Germany). Each batch of samples using the denitrifier method included two international standards (USGS34: $\delta^{15}N$ = -1.8‰ vs N_2, $\delta^{18}O$ = -27.9‰ vs. VSMOW; IAEA-NO-3: $\delta^{15}N$ = 4.7‰ vs N_2, $\delta^{18}O$ = +25.6‰ vs. VSMOW) (Böhlke et al., 2003) and an internal standard. A bracketing correction (Sigman et al., 2009) was applied to the nitrate isotope data to correct for exchange with water. To calibrate $\delta^{15}N\text{-}NH_4^+$ measurements, three international standards (IAEA-N-1: $\delta^{15}N$ = 0.4‰, USGS25: $\delta^{15}N$ = -30.4‰, USGS26: $\delta^{15}N$ = 53.7‰) were used with each sample run. All measurements were replicated, with a typical reproducibility for $\delta^{15}N\text{-}NO_3^-$, $\delta^{18}O\text{-}NO_3^-$

and $\delta^{15}N\text{-}NH_4^+$ better than 0.2‰, 0.6‰ and 0.9‰, respectively. Since NO_2^- comprised on average 2% of the combined NO_2^- + NO_3^- pool, the contribution of NO_2^- interference to the reported $\delta^{15}N$ and $\delta^{18}O$ nitrate values was considered negligible.

N and O isotope ratios are reported in per mil (‰), relative to the analytical standards (N_2 in air for $\delta^{15}N$, and Vienna Standard Mean Ocean Water (VSMOW) for O) using Eq. (1).

3.4 C and N recycling rates

Depth-integrated rates (total rate per unit area) of POC oxidation to DIC ($RPOC_{TOT}$, mmol C m^{-2} d^{-1}), ammonification of particulate organic N (R_{AMF}, mmol N m^{-2} d^{-1}), nitrification of NH_4^+ to NO_3^- (R_{NIT}, mmol N m^{-2} d^{-1}) and denitrification of NO_3^- to N_2 (R_{DEN}, mmol N m^{-2} d^{-1}) were calculated using a mass balance of the fluxes (F) of O_2, NO_3^- and NH_4^+ measured in the benthic chambers (Dale et al., 2014):

$$RPOC_{TOT} = \frac{r_{CN}\,(2\,F_{NH4}\,r_{NO3} - F_{O2}\,r_{NO3} - F_{NH4}\,r_{O2} - F_{NO3}\,r_{O2})}{2\,r_{NO3} - r_{O2} + r_{CN}\,r_{NO3}\,r_{O2}} \quad (2)$$

$$R_{AMF} = \frac{RPOC_{TOT}}{r_{CN}} \quad (3)$$

$$R_{NIT} = \frac{-F_{O2}\,r_{NO3} - F_{NO3}\,r_{O2} - F_{NH4}\,r_{CN}\,r_{NO3}\,r_{O2}}{2\,r_{NO3} - r_{O2} + r_{CN}\,r_{NO3}\,r_{O2}} \quad (4)$$

$$R_{DEN} = \frac{-F_{O2} - F_{NH4}\,r_{CN}\,r_{O2} - 2\,F_{NO3} - F_{NO3}\,r_{CN}\,r_{O2}}{2\,r_{NO3} - r_{O2} + r_{CN}\,r_{NO3}\,r_{O2}} \quad (5)$$

where r_{CN} is the atomic C:N ratio in organic matter undergoing degradation, and r_{O2} and r_{NO3} are the molar ratios of O_2:POC and NO_3^-:POC, respectively, during aerobic respiration and denitrification of organic carbon. r_{O2} and r_{NO3} were previously defined as 118/106 and 94.4/106 (respectively) for organic matter with an oxidation state of -0.45 (Dale et al., 2014). These equations are only approximations because they ignore NO_2^- fluxes, yet which are equivalent to only a few percent of NO_3^- fluxes.

3.5 Isotope calculations

The loss of NO_3^- inside the chambers due to benthic respiration takes place within a closed system where there is no exchange of NO_3^- with the surrounding waters. Under these conditions, the apparent benthic fractionation of N ($^{15}\epsilon_{app}$) or O ($^{18}\epsilon_{app}$) was calculated using a closed system Rayleigh model (Marioitti et al., 1981; Prokopenko et al., 2013):

$$\delta^H X - \delta^H X_0 = {}^{-H}\epsilon_{app}\,ln\,f \quad (6)$$

where $\delta^H X$ and $\delta^H X_0$ denote the isotopic composition (‰) of X (N or O) during the incubation and at the start of the incubation, respectively, and f is the remaining fraction of NO_3^- in the chamber. $^H\epsilon_{app}$ is equal to the slope of the linear regression of a plot of $\delta^H X$ versus $\ln(f)$. Values of ϵ_{app} at each station were determined by pooling the data from both BIGO chambers. Only slopes that were significant (p value< 0.05) are reported, which eliminates the $^{15}\epsilon_{app}$ and $^{18}\epsilon_{app}$ data from the two deepest stations and also $^{18}\epsilon_{app}$ from St. 3 and 7. At these sites, the change in $\delta^H X$ is too small or scattered to calculate reliable ϵ_{app}.

$^H\epsilon_{app}$ is related to the $\delta^H X$ of the NO_3^- flux relative to the $\delta^H X$ of bottom water NO_3^-, $\delta^H X_{NO_{3BW}}$ (Alkhatib et al., 2012):

$${}^H\epsilon_{app} = \delta^H X_{NO_{3_{BW}}} - \delta_{F_{NO_3}} \quad (7)$$

Where

$$\delta_{F_{NO_3}} = \left(\frac{\left(F_{H_{NO_3}}/F_{L_{NO_3}}\right)}{\left({}^H\mathrm{N}/{}^L\mathrm{N}\right)_{\mathrm{Standard}}} - 1 \right) \cdot 1000 \quad (8)$$

and $F_{H_{NO3}}$ and $F_{L_{NO3}}$ are the benthic fluxes of the heavy and light isotopologues at the sediment surface, respectively (see Supplement).

4 Results

4.1 Particulate geochemistry across the margin

Mean POC content in the sediment cores retrieved by the MUC increased from < 1% on the shelf (< 200 m) to 2.9% at the deepest station (Table 1). $CaCO_3$ showed maximum values at St. 4 (37%) and decreased offshore. POC content was significantly and positively correlated with the particulate mud fraction (MF, %) reported by Dale et al. (2014), where POC = 28.1 MF – 13.3 (p< 0.05, data not shown) whereas $CaCO_3$ was not. The mean $\delta^{13}C$ and $\delta^{15}N$ of the particulate material close to St. 5 was -20.8 ± 0.2 ‰ and 3.7 ± 0.4 ‰, respectively (see Supplement). These $\delta^{13}C_{POC}$ fall within the range of -16 to -22 ‰ characteristic of marine organic matter (Meyers, 1994). The mean atomic ratio of POC to PON (r_{CN}, mol C (mol N)$^{-1}$) in each sediment core was mainly constant over the transect (~9 – 10), with a lower ratio at St. 4 of 7.6. These values are typical for marine algae (Burdige, 2006).

4.2 Seafloor recycling of biogenic matter

NO_3^- fluxes were directed into the sediment with highest values on the shelf (-2.9 mmol m^{-2} d^{-1}) (Table 2). NO_2^- effluxes were highest on the shelf (0.13 mmol m^{-2} d^{-1}) and at least a factor of 20 lower than the NO_3^- flux. NH_4^+ and H_4SiO_4 fluxes

10.3389/fmars.2022.902062

were also highest on the shelf and directed from the sediment to the bottom water (Figure S1). The ratio of Si fluxes relative to DIC was 0.5 ± 0.2 and higher than the diatomic Si:C ratio of 0.13 (Brzezinski, 1985), indicating preferential dissolution of opal compared to POC.

In situ fluxes of O_2, DIC and nutrients were highest on the shelf and lowest offshore (Table 2 and Figure 1A). DIC fluxes (F_{DIC}) decreased from 20.7 mmol m^{-2} d^{-1} at St. 1 to 3.5 mmol m^{-2} d^{-1} at St. 9. O_2 fluxes (= TOU) were on average 25% lower than F_{DIC}. The offshore decrease in F_{DIC} and TOU are consistent with a decrease in remineralization of labile organic matter with increasing water depth. $RPOC_{TOT}$ decreased from 18.2 mmol m^{-2} d^{-1} on the shelf to ~2 mmol m^{-2} d^{-1} at St. 9. $RPOC_{TOT}$ was equal to 82% of F_{DIC} for the margin as a whole (Figure 1B). The excess DIC flux over TOU is likely to be driven by carbonate dissolution induced by metabolically-produced CO_2 in surface sediment (Jahnke and Jahnke, 2004). This is further indicated by the respiratory quotient (RQ), determined as the ratio between DIC outflux and O_2 influx across the sediment surface. RQ was 1.5 ± 0.6 across the margin (Table 2). Whilst similar to other estimates using benthic chambers (Jørgensen et al., 2022), it is much higher than the expected value of 0.7 based on complete aerobic mineralization of organic matter with an average phytoplankton composition (Anderson, 1995).

The sediments acted as a net sink for DIN [NO_3^-+NO_2^-+NH_4^+)]. Denitrification rates (R_{DEN}) decreased from 3.6 mmol N m^{-2} d^{-1} on the shelf where $RPOC_{TOT}$ was highest, to < 1 mmol N m^{-2} d^{-1} at the deepest stations. These are consistent with those determined from ^{15}N labelling experiments (Sokoll et al., 2016). R_{DEN} accounted for 24% of $RPOC_{TOT}$ (Figure 1C). Nitrification (R_{NIT}) was apparently active at every station with rates that were 17% of R_{DEN} on average.

The loss of fixed N was further evident in the flux of the tracer N* (F_{N^*}) (Gruber and Sarmiento, 1997; Lehmann et al., 2004):

$$F_{N*} = F_{DIN} - 16\,F_{PO4} \quad (9)$$

TABLE 1 Mean contents of POC, $CaCO_3$ and the C:N ratio in the sediment cores recovered from each station along with mean bottom water O_2 concentrations recorded on the BIGO landers.

Station	Water depth (m)	O_2 (µM)	$CaCO_3$ (%)	POC (%)	r_{CN} (mol C mol N^{-1})
1	46	40	23	0.8	10.1
2	65	25	22	0.7	8.8
3	90	26	31	0.7	8.9
4	130	40	37	0.9	7.6
5	174	41	27	1.1	9.7
6	241	47	17	0.8	9.1
7	412	42	11	1.3	10.3
8	787	76	13	2.7	9.6
9	1100	116	13	2.9	9.2

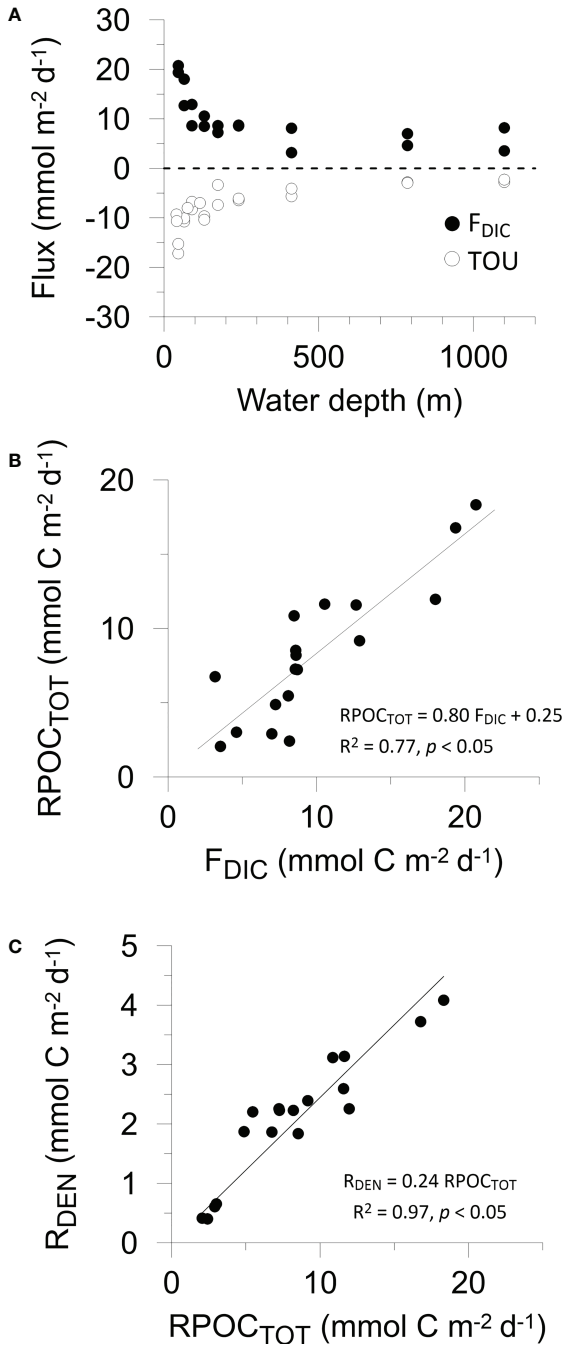

FIGURE 1
(A) Benthic fluxes of DIC (black symbols) and TOU (open symbols) versus water depth. Two data points per water depth correspond to the two benthic chambers in each BIGO lander. Cross plots of **(B)** organic carbon degradation versus measured DIC flux, and **(C)** denitrification versus organic carbon degradation, as determined by the mass balance. Denitrification rates (Table 2) have been converted to mmol C m^{-2} d^{-1} by dividing by r_{NO3}. The trendline in **(C)** has been forced through the origin so that R_{DEN} = 0 if $RPOC_{TOT}$ = 0. For **(B, C)**, Pearson correlation coefficients and *p* values are given.

TABLE 2 Benthic fluxes (F) measured in the individual benthic chambers (mmol m^{-2} d^{-1}) across the transect, the respiratory quotient (RQ, see text) and depth-integrated reaction rates, R [Eq. (2)-(5)].

Station	BIGO		Water depth (m)	F_{DIC}	F_{O_2}	F_{NO_3}	F_{NO_2}	F_{NH_4}	F_{Si}	F_{PO_4}	F_{N^*}	RQ	$RPOC_{TOT}$	R_{AMF}	R_{DEN}	R_{NIT}
1	BIGO 2-4	C1	46	20.7	-17.2	-3.0	0.12	1.14	11.8	0.17	-4.47	1.2	18.3	1.8	3.6	0.7
		C2	46	19.4	-15.3	-2.9	0.09	1.29	11.0	0.24	-5.47	1.3	16.8	1.7	3.3	0.4
2	BIGO 2-5	C1	65	18.0	-10.7	-2.0	0.13	1.39	8.5	0.21	-3.90	1.7	12.0	1.4	2.0	n.d
		C2	65	12.7	-10.1	-2.3	0.11	1.26	7.3	0.15	-3.24	1.3	11.6	1.3	2.3	0.1
3	BIGO 1-3	C1	90	12.9	-8.3	-1.8	0.11	0.66	4.4	0.05	-1.72	1.6	9.2	1.0	2.1	0.4
		C2	90	8.6	-6.8	-2.0	0.06	1.30	4.5	0.13	-2.78	1.3	8.5	1.0	1.6	n.d
4	BIGO 1-4	C1	130	8.5	-9.7	-2.2	0.03	0.89	5.9	0.15	-3.70	0.9	10.9	1.4	2.8	0.5
		C2	130	10.6	-10.4	-2.3	0.06	1.07	7.0	0.17	-3.97	1.0	11.6	1.5	2.8	0.5
5	BIGO 2-3	C1	174	8.6	-7.4	-1.6	0.03	0.47	4.2	0.11	-2.82	1.2	8.2	0.8	2.0	0.4
		C2	174	7.2	-3.4	-1.7	0.06	0.50	4.4	0.17	-3.87	2.2	4.9	0.5	1.7	0.0
6	BIGO 1-2	C1	241	8.6	-6.5	-1.6	0.04	0.37	3.5	0.06	-2.06	1.3	7.3	0.8	2.0	0.4
		C2	241	8.7	-6.1	-1.7	0.04	0.51	3.7	0.16	-3.74	1.4	7.2	0.8	2.0	0.3
7	BIGO 2-2	C1	412	3.2	-5.7	-1.6	0.05	0.55	3.0	0.11	-2.65	0.6	6.8	0.7	1.7	0.1
		C2	412	8.1	-4.1	-1.7	0.02	0.29	1.6	0.06	-2.41	2.0	5.5	0.5	2.0	0.2
8	BIGO 1-1	C1	787	7.0	-2.8	-0.4	0.00	0.18	1.7	0.04	-0.95	2.5	2.9	0.3	0.5	0.1
		C2	787	4.6	-2.9	-0.4	0.00	0.16	1.6	0.05	-1.09	1.6	3.0	0.3	0.6	0.2
9	BIGO 2-1	C1	1100	8.2	-2.8	-0.1	0.00	–	1.7	0.05	-0.74	3.0	2.4	0.3	0.4	0.3
		C2	1100	3.5	-2.3	-0.1	0.00	–	1.5	0.06	-1.37	1.5	2.1	0.2	0.4	0.2
			Mean	9.9	-7.3	-1.6	0.05	0.66	4.8	0.12	-2.83	1.5	8.3	0.9	1.9	0.3
			SD	4.9	4.2	0.8	0.04	0.48	3.1	0.06	1.29	0.6	4.5	0.5	0.9	0.2

Negative fluxes denote uptake by the sediment and vice versa. Negative N* fluxes indicate preferential loss of N relative to P. Mean values ± standard deviation are also given. Cases where the mass balance did not converge (only applicable for R_{NIT}) are listed as not defined (n.d).

where F_{PO4} is the PO_4^{3-} flux (Table 2) and the factor 16 stems from the Redfield composition of organic matter (N:P = 16:1). If organic N and P are completely remineralized, $F_{N^*} = 0$. F_{N^*} was negative at all sites because the sediments acted as a source of PO_4^{3-} and a sink of DIN, illustrating preferential loss of DIN relative to PO_4^{3-}. The most negative N* flux of -5.5 mmol m^{-2} d^{-1} was determined at St. 1 where R_{DEN} was highest. The highest F_{N^*} of -1 mmol m^{-2} d^{-1} was calculated for St. 9. Across the transect, the mean F_{N^*} was -2.8 ± 1.3 mmol m^{-2} d^{-1}.

4.3 N isotopes in benthic chambers

$\delta^{15}N\text{-}NO_3$ and $\delta^{18}O\text{-}NO_3$ inside the benthic chambers are illustrated in Figure 2. Bottom water $\delta^{15}N\text{-}NO_3$, taken as the first time point immediately after the chambers were closed, was approximately 5.0 ± 0.5 ‰. Enrichments in ^{15}N over time were generally observed in all chambers on the shelf and upper slope. $\delta^{15}N\text{-}NO_3$ increased by roughly 1 ‰ on the shelf and by <1 ‰ on the upper slope over the course of the incubations. At the two deepest sites, variations in $\delta^{15}N\text{-}NO_3$ and $\delta^{18}O\text{-}NO_3$ were within analytical precision. Bottom water $\delta^{18}O\text{-}NO_3$ was more variable than $\delta^{15}N\text{-}NO_3$. Enrichments in ^{18}O were stronger on the shelf compared to the slope.

The apparent fractionation of N ($^{15}\epsilon_{app}$) and O ($^{18}\epsilon_{app}$) accompanying NO_3^- loss inside the benthic chambers varied between 0.7 and 2.0 ‰ for $^{15}\epsilon_{app}$ and between 1.7 and 2.9 ‰ for $^{18}\epsilon_{app}$ with no clear trends across the transect (Figure 3A and Table S4). The average $^{15}\epsilon_{app}$ and $^{18}\epsilon_{app}$ were 1.5 ± 0.4 ‰ and 2.0 ± 0.5 ‰, respectively. For the shelf (< 100 m), $^{18}\epsilon_{app}$ was twice as high as $^{15}\epsilon_{app}$ (1.8 versus 0.9 ‰). The ratio of these numbers, $^{18}\epsilon_{app}$:$^{15}\epsilon_{app}$, varied from 2.0 to 2.3 at stations 1, 2 and 4. $^{18}\epsilon_{app}$:$^{15}\epsilon_{app}$ was 0.9 at St. 5 and 6 (Figure 3B). The mean $^{18}\epsilon_{app}$:$^{15}\epsilon_{app}$ ratio of the shelf stations was 2.1 ± 0.3.

$\delta^{15}N\text{-}NH_4$ inside the benthic chambers at St. 1 and 2 was between 9 and 10 ‰ whereas the values at St. 3 were more scattered (Figure S2). The $\delta^{15}N$ of the NH_4^+ flux out of the sediment to the bottom water (δF_{NH4}) for the shelf stations was calculated as the intercept of a linear regression of $\delta^{15}N\text{-}NH_4$ versus the inverse NH_4^+ concentration (Mortazavi and Chanton, 2004; Dale et al., 2019). Values of δF_{NH4} were similar and varied from 8 ± 1.8 ‰ at St. 1 to 9.6 ± 1.2 ‰ at St. 2 (Figure 3C and Table S4). The average δF_{NH4} of the three shelf sites was 9.0 ± 0.7 ‰.

5 Discussion

5.1 N cycling inferred from benthic chamber isotopes

The increase in $\delta^{15}N\text{-}NO_3$ and $\delta^{18}O\text{-}NO_3$ in the benthic incubation chambers, along with a decrease in NO_3^-

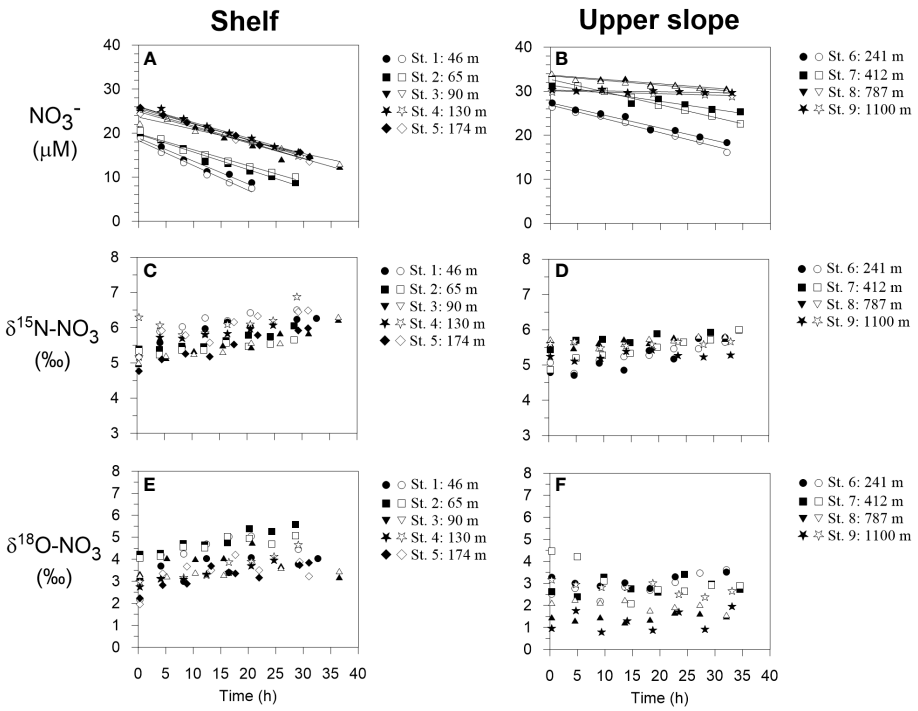

FIGURE 2
Benthic chamber incubation results for NO_3^- on the shelf and upper slope. **(A, B)** NO_3^- concentrations with linear regression curves from which the fluxes are calculated, **(C, D)** $\delta^{15}N\text{-}NO_3$ and **(E, F)** $\delta^{18}O\text{-}NO_3$. Filled and open symbols correspond to chamber 1 and 2 during each BIGO lander deployment, respectively.

concentrations, is attributed to dissimilatory reduction of NO_3^- to NO_2^- (Lehmann et al., 2004; Dale et al., 2014; Dale et al., 2019). Isotope effects for nitrate reduction estimated from $\delta^{15}N\text{-}NO_3$ distributions in the water column are ca. 15 – 30 ‰ (Voss et al., 2001; Kritee et al., 2012; Bourbonnais et al., 2015) for both ^{15}N and ^{18}O (Marioitti et al., 1981; Voss et al., 2001; Casciotti et al., 2002; Granger et al., 2008; Kritee et al., 2012). Thus, our data would appear to present two conflicts with the known isotopic fingerprint of dissimilatory NO_3^- reduction: (i) the apparent benthic fractionation factors, $^{15}\epsilon_{app}$ and $^{18}\epsilon_{app}$, are much lower than observed in the water column at all sites, and (ii) the ratio $^{18}\epsilon_{app}$:$^{15}\epsilon_{app}$ is higher than unity at St. 1, 2 and 4, but closer to unity at St. 5 and 6 (Figure 3).

On continental margins, including Mauritania, NO_3^- is typically exhausted within a few centimeters below the sediment surface due to high rates of respiration by microorganisms (Dale et al., 2014). The strong drawdown of NO_3^- leads to diffusive transport limitation of NO_3^- to the subsurface denitrifying layer, leading to complete consumption of NO_3^- that diffuses into the sediment (Brandes and Devol, 1997). This results in an under-expression of the isotope effect in the benthic NO_3^- flux and explains why larger isotope effects are observed in the water column (Brandes and Devol, 1997; Brandes and Devol, 2002; Lehmann et al., 2007; Alkhatib et al., 2012; Dale et al., 2019). The range of $^{15}\epsilon_{app}$ determined in this study is similar to that reported for other coastal sediments under oxygenated waters (Brandes and Devol, 2002; Lehmann et al., 2007; Alkhatib et al., 2012). ϵ_{app} may be larger in oxygen-deficient regions because the distance for molecules to diffuse between the seawater NO_3^- reservoir and the denitrification layer is smaller (Brandes and Devol, 1997; Lehmann et al., 2007). For instance, $^{15}\epsilon_{app}$ of 6 ± 2 ‰ were observed in sediments under hypoxic bottom waters in the Bering Sea (Lehmann et al., 2007). Sediments underlying anoxic waters in the Peruvian OMZ displayed even higher $^{15}\epsilon_{app}$ of 7.4 ± 0.7 ‰, decreasing to 2.5 ± 0.9 ‰ under oxygenated waters below the OMZ, with similar trends in $^{18}\epsilon_{app}$ (Dale et al., 2019). Dähnke and Thamdrup (2013) measured $^{15}\epsilon_{app}$ and $^{18}\epsilon_{app}$ of 18.9 ‰ and 15.8 ‰, respectively, in anoxic ex-situ incubations of organic-rich sediment. These results confirm observations and model predictions that nitrate isotope effects inferred from benthic flux data are under-expressed under oxic waters (Brandes and Devol, 1997; Lehmann et al., 2004; Lehmann et al., 2007). However, the assumption of a universally low or negligible benthic N isotope effect, as originally predicated in earlier studies, is not fully applicable to oxygen-deficient settings (Brandes and Devol, 1997; Lehmann et al., 2004).

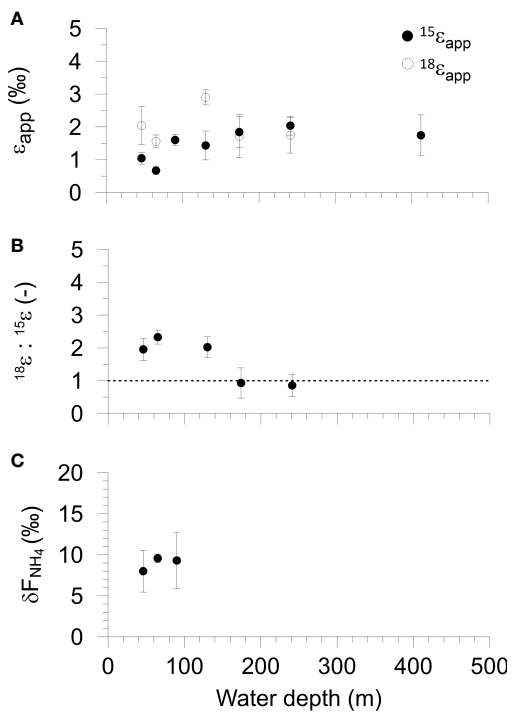

FIGURE 3
Benthic chamber isotope results versus water depth on the Mauritanian margin. **(A)** Fractionations of N-NO_3^- ($^{15}\epsilon_{app}$) and O-NO_3^- ($^{18}\epsilon_{app}$). **(B)** The ratio $^{18}\epsilon_{app}$: $^{15}\epsilon_{app}$, where the dashed line shows unity. **(C)** The $\delta^{15}N$ of the NH_4^+ flux from the sediment. Error bars represent the standard error of the regression slopes (see Methods). Data are tabulated in Table S1 in the Supplement.

$^{15}\epsilon_{app}$ and $^{18}\epsilon_{app}$ were substantially lower than the values of 8 and 14 ‰, respectively, determined in a single chamber at St. 1 in 2011 (Dale et al., 2014). While some temporal variability is to be expected, the difference between 2011 and 2014 is as much striking as it is puzzling, because the redox conditions and fluxes were not radically different. Lower O_2 levels in 2011 are unlikely to be the cause (see Section 5.3). $\delta^{15}N$-NO_3 and $\delta^{18}O$-NO_3 were measured in 2011 using the Cd-reduction/azide method with addition of NaCl (Ryabenko et al., 2009) and verified against the same international standards USGS34 and IAEA-NO-3. In 2011, the BIGO samples for isotope analysis were taken in quartz tubes whereas in 2014 the syringe samples were used (see Methods). The quartz tube samples were first analyzed on board for dissolved gases by passing the sample (without air contact) through the membrane inlet of a mass spectrometer prior to filtering and freezing. It is currently unclear whether this procedure significantly altered the isotopic composition of NO_3^-. Unfortunately, additional samples from the syringes were not analyzed during the 2011 campaign for comparison, and we are presently unable to resolve the inter-annual differences in $^{15}\epsilon_{app}$ and $^{18}\epsilon_{app}$.

A more realistic estimate of the total benthic N isotope effect on the oceanic N reservoir can be made from the flux of all fixed N species across the sediment-water interface, termed ϵ_{sed} by Lehmann et al. (2007). $^{15}\epsilon_{sed}$ can be higher than $^{15}\epsilon_{app}$ in continental margins if the sediment acts as a source of ^{15}N-enriched NH_4^+ to the water column, which in our setting has a $\delta^{15}N$ of ~9.0 ‰ (Figure 3C). Vertical mixing and oxidation of ^{15}N-enriched NH_4^+ higher up in the water column will then increase the $\delta^{15}N$ of the ocean NO_3^- reservoir. Mathematically, $^{15}\epsilon_{sed}$ can be calculated as:

$$^{15}\epsilon_{sed} = \delta^{15}N_{NO_{3_{BW}}} - \delta_{J_{Nreac}} = \delta^{15}N_{NO_{3_{BW}}} - \delta_{J_{N2}} \quad (10)$$

where $\delta_{J_{Nreac}}$ is the $\delta^{15}N$ of the net flux of reactive N species (NO_3^-, NO_2^-, NH_4^+, PON) and $\delta_{J_{N2}}$ is the $\delta^{15}N$ of all fixed N lost to N_2 ($\delta_{J_{N2}}$). This expression ignores dissolved organic nitrogen, which may be important in some settings (Alkhatib et al., 2012). Alkhatib et al. (2012) used a similar approach to determine $^{15}\epsilon_{app}$ based on NO_3^- fluxes (Eq. 7). Accurate estimations of $^{15}\epsilon_{sed}$ are hampered by the fact that $\delta_{J_{Nreac}}$ requires accurate isotope values for the fixed N fluxes including PON remineralization (Dale et al., 2019). Similarly, precise analytical determination of $\delta_{J_{N2}}$ is difficult due to the large background reservoir of N_2 in seawater (Brandes and Devol, 1997). In the following section, $^{15}\epsilon_{sed}$ is estimated using a numerical model of the benthic chamber incubation.

Deviations of $^{18}\epsilon_{app}$:$^{15}\epsilon_{app}$ above 1 are generally interpreted as the superimposition of the kinetic isotope effects of nitrification of NH_4^+ and denitrification (e.g. Lehmann et al., 2004; Dale et al., 2014). NH_4^+ is initially released to the porewater by the ammonification of PON with a small KIE of 1 – 2 ‰ (Möbius, 2013). The $\delta^{15}N$ of PON in the upper 30 cm of sediment on the margin is ~ 5 ‰ (Table S1). Hence, the $\delta^{15}N$ of NH_4^+ from ammonification should be close to this value. By contrast, nitrification of NH_4^+ to NO_2^- is associated with a large kinetic N isotope effect of 14 – 38 ‰ (Marioitti et al., 1981; Casciotti et al., 2003). The mass balance ($R_{NIT}/R_{AMF} < 1$) and the ^{15}N-enriched NH_4^+ effluxes indicate that NH_4^+ is only partially nitrified. If newly nitrified and ^{15}N-depleted NO_2^- is quantitatively oxidized to NO_3^-, the ^{15}N-depleted NO_3^- will dilute the ambient porewater NO_3^- pool with $^{14}NO_3^-$ and counteract the loss of $^{14}NO_3^-$ incurred through dissimilatory reduction (Lehmann et al., 2004; Lehmann et al., 2007). Nitrification does not lead to a similar behavior of $^{18}\epsilon_{app}$ because the $\delta^{18}O$ of newly nitrified NO_3^- is largely set by the $\delta^{18}O$ of seawater and is equal to ca. 0 ‰ (Buchwald and Casciotti, 2010; Casciotti et al., 2010; Buchwald et al., 2012). In other words, the $\delta^{15}N$ of NO_3^- in porewater subject to denitrification and partial nitrification will increase less quickly than its $\delta^{18}O$ signature, as long as the isotope effects for N and O by nitrate reduction are equivalent, leading to $^{18}\epsilon_{app}$:$^{15}\epsilon_{app}$.

The isotopic fingerprints of partial nitrification must be communicated back to the overlying chamber water in order

to bring about a change in observed $^{18}\epsilon_{app}$:$^{15}\epsilon_{app}$. This could take place directly by the injection of NO_3^- from the porewater into the chamber through flushing of animal burrows (Lehmann et al., 2004; Dale et al., 2014; Rooze and Meile, 2016), or indirectly by the alteration of the concentration gradients of NO_3^- isotopes at the sediment-water interface and subsequent changes in diffusive fluxes of individual isotopes (Bender, 1990; Brandes and Devol, 1997). All other things being equal, the combined effects of denitrification and partial nitrification ought to lead to $^{18}\epsilon_{app}$:$^{15}\epsilon_{app}$ values above 1 (Lehmann et al., 2004; Dale et al., 2014).

The turnover of NO_2^- adds an additional dimension to the N cycle that has received far more attention in the water column compared to sediments (Casciotti and McIlvin, 2007; Casciotti et al., 2013; Granger and Wankel, 2016). Reduction of NO_2^- occurs with a normal KIE (Casciotti et al., 2002), whereas NO_2^- oxidation occurs with an inverse KIE in both N and O, leaving residual NO_2^- depleted in ^{15}N and ^{18}O (Casciotti, 2009; Buchwald and Casciotti, 2010). Concurrent nitrate reduction and nitrite oxidation can lead to an enrichment of ^{15}N in the ambient NO_3^- pool and an enrichment of ^{14}N in NO_2^-. Several lines of evidence based on NO_2^- isotopes suggest that a significant fraction of NO_2^- produced by nitrate-reducing bacteria in oxygen deficient waters is reoxidized to NO_3^-, resulting in the $\delta^{15}N$ of NO_2^- being up to 60 ‰ lower than coexisting NO_3^- (Casciotti and McIlvin, 2007; Casciotti et al., 2013). A comprehensive box model of N and O isotope dynamics in the water column has since shown that the extent to which NO_3^- is produced relative to the fraction that is reduced plays a central role in determining the trajectories of $\delta^{15}N$-NO_3^- and $\delta^{18}O$-NO_3^- and hence $^{18}\epsilon_{app}$:$^{15}\epsilon_{app}$ (Granger and Wankel, 2016). The relevance of NO_2^- for benthic N fractionation and $^{18}\epsilon_{app}$:$^{15}\epsilon_{app}$ trajectories has been largely unexplored in benthic N isotope studies. In the following, we examine NO_2^- cycling in sediments more closely using a numerical model.

5.2 Insights from model simulations of a benthic chamber incubation experiment

5.2.1 Model set-up and calibration

In this section, we set up a multi-process numerical model of dual N and O isotope dynamics. The model consists of a 1-D, vertically-resolved, reaction-transport model of the surface sediment (upper 12 cm) coupled to a single box representative of a virtual benthic chamber, similar to the one described by Dale et al. (2019) for the Peruvian shelf. In this first step, the model is parameterized using data from St. 2 to constrain key model parameters and fractionations of the benthic N cycle for the Mauritanian shelf. In the second step, we apply the model more generally to explore the sensitivities of $^{18}\epsilon_{app}$:$^{15}\epsilon_{app}$ ratios toward different pathways of N turnover. We also interrogate the impact of the ^{15}N-enriched NH_4^+ efflux on the benthic N isotope effect on water column NO_3^-. Since most of the model structure and reaction network have been described elsewhere, we relegate the bulk of the corresponding model details to the Supplement, and here we only discuss the relevant aspects for this study (Bohlen et al., 2011; Dale et al., 2019).

The degradation of POC in the sediment drives the benthic N cycle, which in turn impacts the concentrations of N species and their isotopes in the benthic chamber. No N cycling is assumed to take place in the benthic chamber water, such that the measured chamber data act as passive tracers for the processes taking place in the sediment. The model includes most of the processes in the water column box model of Granger and Wankel (2016), including aerobic NH_4^+ oxidation (AMO), NO_3^- reduction (NAR), aerobic NO_2^- oxidation (NXR), and NO_2^- reduction to N_2 (NIR). In our model, NAR and NIR are coupled to the degradation of POC. Other electron acceptors for POC remineralization include O_2 and sulfate (SO_4^{2-}). The transition from one metabolic pathway to another during POC respiration depends on the relative concentrations of the terminal electron acceptors (TEA) and user-defined TEA threshold concentrations akin to half-saturation constants (Jourabchi et al., 2005). The TEAs are consumed in the order O_2: NO_2^-: NO_3^-: SO_4^{2-}, such that a high concentration of a TEA will inhibit less-favorable metabolic pathways. We also include ammonification of PON (AMF) that is linked to POC degradation through the atomic C:N ratio of organic matter. NH_4^+ and NO_2^- oxidation during AMO and NXR are defined as second-order reactions with rate constants k_{AMO} and k_{NXR}, respectively. At this stage, we do not consider anammox as it is a minor N loss pathway on the margin (Sokoll et al., 2016). We later relax this assumption for the sensitivity analysis. Solutes are able to diffuse through the porewater and across the sediment-water interface into and out of the benthic chamber depending on the reactions taking place in the sediment. Solute transport is also affected by bioirrigation, expressed mathematically as a simple non-local mixing function, and by bioturbation, expressed as a diffusion-like process.

The rate of organic matter degradation typically decreases with depth in the sediment as it becomes more recalcitrant over time (Middelburg, 1989). This can be constrained by the corresponding increase in NH_4^+ and total alkalinity concentrations (e.g. Berner, 1980). However, these analytes are of limited use to determine POC degradation on the Mauritanian shelf because porewaters are intensively irrigated with seawater by tube-dwelling animals (Gier et al., 2017). Therefore, following Stolpovsky et al. (2015), we used an empirical power law function to parameterize POC mineralization as function of sediment depth, x, termed RPOC(x):

$$\mathrm{RPOC}(x) = 0.5 \cdot (B_1 + x)^{B_2} \quad (11)$$

where RRPOC is the rain rate of POC to the seafloor (in mmol m^{-2} d^{-1}). Comparisons can be drawn between Eq. (11) and the power model proposed by Middelburg (1989) where the rate

constant for POC remineralization depends on the age of POC being degraded. If RRPOC provides an upper limit of the total amount of POC available for degradation, B1 can be defined as:

$$B_1 = (-2 \cdot (B_2 + 1) \cdot RRPOC)^{\frac{1}{1+B_2}} \quad (12)$$

The value of B2 was determined empirically by simulating a global dataset of benthic O_2 and NO_3^- fluxes (Stolpovsky et al., 2015):

$$B_2 = -3.73 \cdot RRPOC^{-0.17} \quad (13)$$

We assigned a value of 16.7 mmol m^{-2} d^{-1} to RRPOC, based partly on the measured TOU and partly on achieving a good fit to the benthic chamber NH_4^+ and NO_3^- fluxes. This gives B_1 and B_2 values of 0.76 cm and -2.3 (dimensionless), respectively.

The KIEs associated with nitrogen cycling (ϵ_{AMO}, ϵ_{NAR}, ϵ_{NIR}, ϵ_{NXR}), the TEA threshold NO_3^- and NO_2^- concentrations during NAR and NIR (K_{NAR}, K_{NIR}) and the rate constants k_{AMO} and k_{NXR} were mainly constrained by fitting the model to the benthic chamber data and, to a lesser extent, to the porewater data (see Supplement Figure S3). All other model parameters were fixed at reasonable values for fine grained shelf sediments, or values derived from field observations. Following Granger and Wankel (2016), we assumed that $^{15}\epsilon_{NAR} = {}^{18}\epsilon_{NAR}$, $^{15}\epsilon_{NIR} = {}^{18}\epsilon_{NIR}$, and $^{15}\epsilon_{NXR} \neq {}^{18}\epsilon_{NXR}$. The $\delta^{15}N$ of NH_4^+ produced from PON was assigned a value of 5 ‰, which is close to the mean $\delta^{15}N$ of oceanic NO_3^- (Brandes and Devol, 2002). The $\delta^{18}O$ of the NO_2^- produced by AMO was fixed (-2.3 ‰, see Supplement) and calculated as a function of the $\delta^{18}O$ of ambient H_2O and O_2, and the fractionation factors associated with their incorporation into NO_2^- (Casciotti et al., 2010). Similarly, the $\delta^{18}O$ of the NO_3^- produced by NXR was set by the inverse O isotope effect of NO_2^- oxidation ($^{18}\epsilon_{NXR}$) and the isotope effect of O incorporation into NO_2^- from water (Buchwald and Casciotti, 2010). In addition to NXR and NIR, the $\delta^{18}O$ of the NO_2^- pool is affected by the branching isotope effect of O atom extraction during NAR ($^{18}\epsilon_{NARBR}$), which was assigned a value of 25 ‰ (Granger and Wankel, 2016). In contrast to observations in the water column, we assumed that the O atoms in NO_2^- are not equilibrated with water (Buchwald and Casciotti, 2013). This is because the abiotic equilibration time is days to weeks (Buchwald and Casciotti, 2013), whereas the residence time of NO_2^- in shelf porewaters in our simulations is typically on the order of minutes. In deep-sea sediments, where NO_2^- turnover rates are far lower, abiotic equilibration must be considered (Buchwald et al., 2018).

As with most ecological models, ours is underdetermined with respect to the number of field observations available to constrain the unknown parameter values. The lack of $\delta^{15}N$ and $\delta^{18}O$ data for NO_2^- from the benthic chambers unfortunately compromises the accuracy of the model simulations. To reduce the margin of error, we ran the model using a Monte Carlo procedure to find the optimum fit to the chamber data by tuning the nine unknown parameters to the benthic chamber data. The model was run over an ensemble of 20 k iterations, in each case with a random set of parameter values chosen from typical ranges reported in the literature (Dale et al., 2014). The parameter values from simulations meeting a least squares criterion for the fit between the model and the benthic chamber data were then averaged. These are listed in Table 3 along with other model outputs of interest including ratios of depth-integrated rates and benthic isotope effects.

The optimized isotope effects for ϵ_{AMO} (35 ± 3 ‰), ϵ_{NAR} (9 ± 3 ‰), ϵ_{NIR} (14 ± 6 ‰), $^{15}\epsilon_{NXR}$ (-8 ± 5 ‰) and $^{18}\epsilon_{NXR}$ (-7 ± 5 ‰) are well-within ranges of previously-determined isotope effects in the water column (reviewed by Granger and Wankel, 2016) and sediments (Lehmann et al., 2007; Alkhatib et al., 2012; Dale et al., 2014; Dale et al., 2019). The best-fit model solutions (n = 54) of the chamber data agree well with the measured data (Figure 4). Modeled $\delta^{15}N$-NO_2^- and $\delta^{18}O$-NO_2^- are clearly sensitive to the set of best-fit parameters. This suggests that NO_2^- isotope data would help to narrow the parameter uncertainty in Table 3. It is interesting that the $\delta^{18}O$-NO_2^- flux is always positive (mean = 27 ± 6 ‰). This is explained by (i) the $\delta^{18}O$ of newly nitrified NO_2^- is set by the $\delta^{18}O$ of seawater, (ii) $^{18}\epsilon_{NIR} > {}^{18}\epsilon_{NXR}$, which enriches porewater NO_2^- in ^{18}O, and (iii) only a small fraction of NO_2^- is reoxidized to NO_3^- (NXR/NAR = 9%). In contrast, the $\delta^{15}N$ of newly nitrified NO_2^- (mean = -3 ± 5 ‰) can be positive or negative because it depends on ϵ_{AMO} and the fraction of NH_4^+ that is oxidized. The $\delta^{15}N$ of the NO_2^- flux is more sensitive to ϵ_{AMO} than any other model parameter (not shown), with higher ϵ_{AMO} leading to more ^{15}N-depleted NO_2^- fluxes.

The model predicts that 14% of NH_4^+ produced from PON is oxidized to NO_2^- (AMO/AMF). This is higher than predicted by the mass balance (RNIT/RAMF ~7%, Table 2), yet necessary in order to reproduce the efflux of ^{15}N-enriched NH_4^+. The disagreement with the model and mass balance may be rooted in the fact that the latter does not explicitly consider NO_2^-. A better agreement between the model and the mass balance was found for denitrification, with the model predicting a fixed N loss of 2.0 ± 0.1 mmol m^{-2} d^{-1}.

The N and O isotope effects for NO_3^- reduction ($^{15}\epsilon_{app}$ = 0.8 ± 0.3 ‰, $^{18}\epsilon_{app}$ = 1.2 ± 0.4 ‰) and the ratio $^{18}\epsilon_{app}$:$^{15}\epsilon_{app}$ (1.8 ± 0.8 ‰) are within the uncertainty of the observed values (Figure 3). In sediments, high $^{18}\epsilon_{app}$:$^{15}\epsilon_{app}$ are thus possible at low NXR/NAR, whereas in the water column elevated $^{18}\epsilon_{app}$:$^{15}\epsilon_{app}$ are associated with NXR/NAR of >50% (Casciotti et al., 2013; Granger and Wankel, 2016). This discrepancy probably arises from the abundance of NH_4^+ in porewaters produced by anaerobic remineralization pathways, mainly sulfate reduction, such that only a small amount of NH_4^+ oxidation with a high ϵ_{AMO} is needed to produce large $^{18}\epsilon_{app}$:$^{15}\epsilon_{app}$ trajectories. In the water column, NH_4^+ production is stoichiometrically constrained by organic matter remineralization using O_2, NO_2^- and NO_3^-, and elevated $^{18}\epsilon_{app}$:$^{15}\epsilon_{app}$ are only feasible with tightly coupled NO_2^- oxidation and NO_3^- reduction.

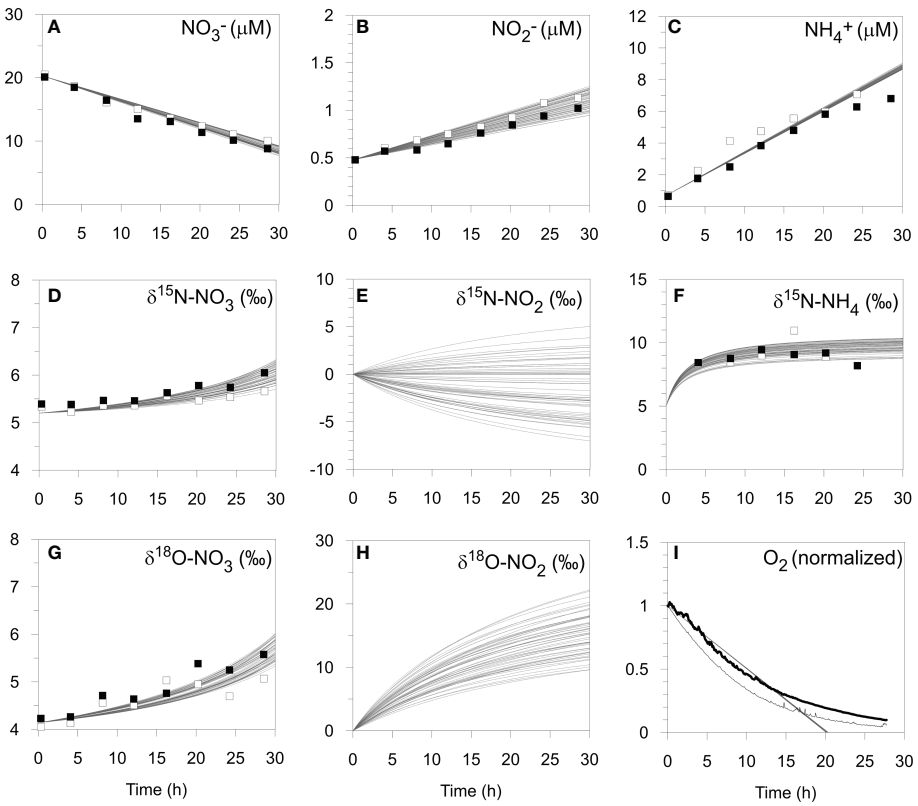

FIGURE 4
Model simulation results (curves, n = 54) of the benthic chamber incubation experiment at St. 2 on the shelf (BIGO 2-5) including **(A–C)** N concentrations, **(D–H)** N and O isotopes, and **(I)** O_2 concentrations (see text). Open and filled symbols correspond to chamber 1 and 2, respectively. For the O_2 optode data, chamber 1 and 2 are denoted by the thin and thick black lines, respectively, and have been normalized to the initial values.

TABLE 3 Key model results for the Mauritanian shelf [a].

Term	Description	Value
ϵ_{AMO}	N isotope effect for aerobic NH_4^+ oxidation, ‰	35 ± 3
$^{15}\epsilon_{NAR}$, $^{18}\epsilon_{NAR}$	N and O isotope effect for NO_3^- reduction, ‰	9 ± 3
$^{15}\epsilon_{NIR}$, $^{18}\epsilon_{NIR}$	N and O isotope effect for NO_2^- reduction, ‰	14 ± 6
$^{15}\epsilon_{NXR}$	N isotope effect for nitrite oxidation, ‰	-8 ± 5
$^{18}\epsilon_{NXR}$	O isotope effect for nitrite oxidation, ‰	-7 ± 5
$^{15}\epsilon_{app}$	Apparent benthic fractionation of N for NO_3^-, ‰	0.8 ± 0.3
$^{18}\epsilon_{app}$	Apparent benthic fractionation of O for NO_3^-, ‰	1.3 ± 0.4
$^{18}\epsilon_{app}$:$^{15}\epsilon_{app}$	Ratio of $^{18}\epsilon_{app}$ to $^{15}\epsilon_{app}$, –	1.7 ± 0.8
$^{15}\epsilon_{sed}$	Total benthic fractionation of N, ‰	3.6 ± 0.5
K_{NAR}	NO_3^- threshold concentration for NO_3^- reduction, μmol cm^{-3}	0.007 ± 0.005
K_{NIR}	NO_2^- threshold concentration for NO_2^- reduction, μmol cm^{-3}	0.006 ± 0.002
k_{AMO}	Rate constant for aerobic NH_4^+ oxidation, cm^3 μmol^{-1} yr^{-1}	$9\times10^5 \pm 1\times10^5$
k_{NXR}	Rate constant for aerobic nitrite oxidation, cm^3 μmol^{-1} yr^{-1}	$6\times10^6 \pm 3\times10^6$
NXR/NAR	NO_3^- production relative to reduction, %	9 ± 5
AMO/AMF	NH_4^+ oxidation relative to production, %	14 ± 1

[a]All model parameters are given in the Supplementary Information.

It is noteworthy that ϵ_{NAR} is much higher than $^{15}\epsilon_{app}$, confirming that the intrinsic cellular fractionation of NO_3^- reduction is not fully expressed in the benthic NO_3^- flux (Lehmann et al., 2007). ϵ_{NAR} is similar to 10 - 15 ‰ determined in pure cultures of denitrifying bacteria under typical marine conditions (Kritee et al., 2012) and to estimates from our previous box model of shelf sediments (~13 ‰, Dale et al., 2014). It also fits well with modelled data from the North Atlantic and Eastern Tropical North Pacific water column (14 ± 2 ‰, Granger and Wankel, 2016). Others have reported comparable values using model approaches that account for both closed and open system effects of NO_3^- reduction on ϵ_{NAR} (Deutsch et al., 2004; Altabet, 2007).

The total benthic N isotope effect, $^{15}\epsilon_{sed}$, calculated using Eq. (10), equals 3.6 ± 0.5 ‰. As expected, it is higher than $^{15}\epsilon_{app}$ because of the efflux of ^{15}N-enriched NH_4^+. The NO_2^- flux, although acting to decrease $^{15}\epsilon_{sed}$, hardly affects $^{15}\epsilon_{sed}$ in this setting since the flux is relatively small (Table 2). The modelled $^{15}\epsilon_{sed}$ is consistent with values of 2 – 6 ‰ determined from porewater gradients in the upper St. Lawrence Estuary where O_2 levels are below 100 µM (Alkhatib et al., 2012). It is also close to estimates of 4 – 7 ‰ reported by Lehmann et al. (2007) for the upper continental margin and with results from a global N isotope model (2 – 4 ‰; Somes et al., 2013).

The environmental controls on $^{15}\epsilon_{sed}$ are not well understood presently, and correlations between $^{15}\epsilon_{sed}$ and organic matter quality and bottom water O_2 levels have been discussed (Lehmann et al., 2007; Alkhatib et al., 2012; Dale et al., 2019). However, changes in organic matter quality and bottom water redox conditions are often intertwined (Cowie et al., 2014), and their individual contribution to $^{15}\epsilon_{sed}$ has not yet been investigated under laboratory conditions. Furthermore, the relationship between $^{15}\epsilon_{sed}$ and bioirrigation is highly non-linear and far more intricated than the simple mathematical expression of bioirrigation used in our model (Rooze and Meile, 2016). The contribution of dissolved organic N fluxes to $^{15}\epsilon_{sed}$ also deserves to be explored in future studies due to its significance in other organic-rich environments (Alkhatib et al., 2012). Despite these caveats, our results provide supporting evidence that benthic N fractionation on the continental margin exceeds previously assumed values of 0 – 2 ‰ for marine sediments (Brandes and Devol, 2002; Altabet, 2007).

5.2.2 Sensitivity of $^{15}\epsilon_{app}$, $^{18}\epsilon_{app}$:$^{15}\epsilon_{app}$ and ϵ_{sed} to N cycling pathways

We now apply the model to explore the sensitivity of ϵ_{app}, $^{18}\epsilon_{app}$:$^{15}\epsilon_{app}$ and $^{15}\epsilon_{Sed}$ to a broader range of N turnover rates, using the best-fit ϵ values in Table 3. To keep the procedure manageable, parameters associated with the physical environment (e.g. compaction, bioirrigation, boundary conditions) and RPOC(x) were left unchanged. Our primary interest here is on the internal interplay of the N cycle pathways in a continental shelf setting like the Mauritanian margin. Anammox (AMX) is now included to make the model more generic and to test the impact of AMX/AMF on the benthic isotope effect (see Supplement). Fractionations of 24 ‰ ($^{15}\epsilon_{AMXNH4}$) and 16 ‰ ($^{15}\epsilon_{AMXNO2}$) were assigned to NH_4^+ oxidation and NO_2^- reduction, respectively (Brunner et al., 2013). The ^{18}O isotope for NO_2^- reduction ($^{18}\epsilon_{AMXNO2}$) was set equal to $^{18}\epsilon_{NIR}$ (Granger and Wankel, 2016). During AMX, an additional 0.3 moles of NO_2^- are oxidized to NO_3^- per mole of NO_2^- reduced, which accounts for the reduction of inorganic carbon during production of biomass (Strous et al., 1999). NO_2^- oxidation by AMX has an inverse N isotope effect ($^{15}\epsilon_{AMXNO2ox}$) of around -30 ‰ and produces ^{15}N-enriched NO_3^- (Brunner et al., 2013). The $\delta^{18}O$ of the NO_3^- was defined analogously as described above for NXR, assuming that the O isotope effect of NO_2^- oxidation by AMX ($^{18}\epsilon_{AMXNO2ox}$) is equal to $^{18}\epsilon_{NXR}$ (Granger and Wankel, 2016).

Model results show linear and non-linear dependencies of ϵ_{app}, $^{15}\epsilon_{Sed}$ and $^{18}\epsilon_{app}$:$^{15}\epsilon_{app}$ on NXR, AMO and AMX (Figure 5). Over the ranges tested, $^{15}\epsilon_{app}$ is most sensitive to the proportion of NH_4^+ oxidized by AMO and AMX (Figure 5A). $^{15}\epsilon_{app}$ increases steadily with AMX (grey curve), which is due to the production of ^{15}N-enriched NO_3^- by the negative N isotope effect of NO_2^- oxidation. On the contrary, $^{15}\epsilon_{app}$ barely changes when NO_2^- oxidation by AMX is turned off (green curve). The production of ^{15}N-enriched NO_3^- by AMX enhances $^{15}\epsilon_{app}$ in the following way. Addition of $^{15}NO_3^-$ to the porewater slightly weakens the $^{15}NO_3^-$ concentration gradient at the sediment surface relative to $^{14}NO_3^-$, leading to an increase in porewater δ^{15}N-NO_3^- (Figure 6A). The flux of $^{15}NO_3^-$ into the sediment is reduced (relative to $^{14}NO_3^-$) and brings about a lowering of the δ^{15}N of the NO_3^- flux into the sediment (Figure 6B). As a consequence, $^{15}\epsilon_{app}$ increases (Eq. (7)). When NO_2^- oxidation by AMX is turned off, the substrates for AMX (NH_4^+ and NO_2^-) are permanently lost as N_2 with no effect on NO_3^-, which curtails any impact on $^{15}\epsilon_{app}$. A similar effect of AMX is observed for $^{18}\epsilon_{app}$ due to the negative O isotope effect of NO_2^- oxidation (grey curve, Figure 5B), which together with $^{15}\epsilon_{app}$ produces very little change in $^{18}\epsilon_{app}$:$^{15}\epsilon_{app}$ over the ranges of AMX tested (grey curve, Figure 5C). This finding is tentative, but agrees with studies in the water column where AMX fails to explain $^{18}\epsilon_{app}$:$^{15}\epsilon_{app}$ trajectories >1 (Granger and Wankel, 2016). Overall, the model suggests that observed $^{18}\epsilon_{app}$:$^{15}\epsilon_{app}$ trajectories > 1 on the Mauritanian shelf are not easily explainable by anammox alone.

AMO has a different impact on $^{15}\epsilon_{app}$ since NH_4^+ is recycled to NO_2^-, part of which can be oxidized to NO_3^-. At low AMO rates, nitrified NO_2^- is strongly depleted in ^{15}N due to the large N isotope effect, ϵ_{AMO}. The portion of this newly nitrified $^{14}NO_2^-$ that is oxidized to $^{14}NO_3^-$ causes a weakening of the $^{14}NO_3^-$ concentration gradient and a decrease in $^{15}\epsilon_{app}$ (blue curve, Figure 5A). As NH_4^+ becomes more quantitatively consumed (AMO/AMF > ~30%), newly nitrified NO_2^- and NO_3^- are increasingly ^{15}N-enriched, reversing the impact on the NO_3^- concentration gradients and

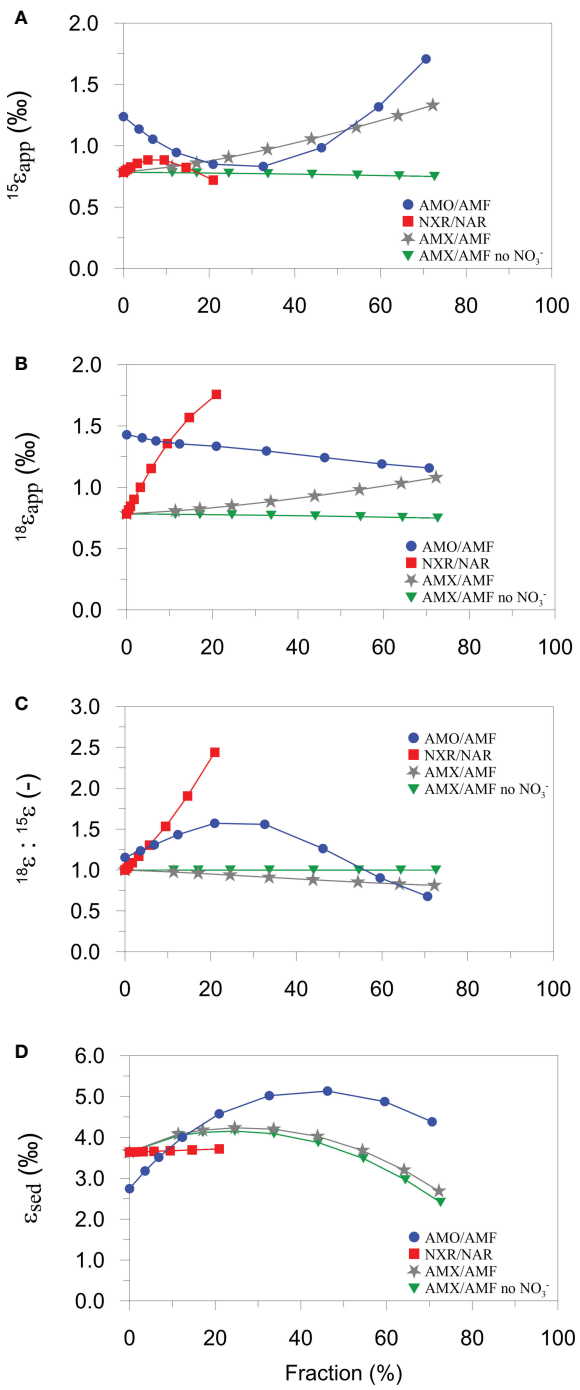

FIGURE 5
Model sensitivity analysis of **(A)** $^{15}\epsilon_{app}$, **(B)** $^{18}\epsilon_{app}$, **(C)** $^{18}\epsilon_{app}$:$^{15}\epsilon_{app}$, and **(D)** $^{15}\epsilon_{sed}$ towards AMO, AMX and NXR, given as percentage contributions to AMF or NAR. Blue, red and grey curves were generated by varying the rate constant for AMO (k_{AMO}), NXR (k_{NXR}), and AMX (k_{AMX}) stepwise between 0 and 2.6 × 10^7 cm^3 μmol^{-1} yr^{-1}. The green curves are the results for AMX/AMF without oxidation of NO_2^- to NO_3^-. All other parameter values in Table 3 and Table S2 are held constant.

producing an increase in $^{15}\epsilon_{app}$. By contrast, $^{18}\epsilon_{app}$ decreases by less than 0.5 ‰ for the full range of AMO/AMF because the $\delta^{18}O$ of newly nitrified NO_2^- is fixed (-2.3 ‰). The N and O effects of AMO combine to give a trajectory in $^{18}\epsilon_{app}$:$^{15}\epsilon_{app}$ that is highest at intermediate values of AMO/AMF (blue curve, Figure 5C). If AMO/AMF exceeds ~60%, $^{18}\epsilon_{app}$:$^{15}\epsilon_{app}$ even falls below 1. Thus, for the present model configuration, AMO can explain a wide range of $^{18}\epsilon_{app}$:$^{15}\epsilon_{app}$ ratios observed in the field.

In contrast to AMO/AMF, the fraction of NO_2^- that is oxidized relative to NO_3^- reduction (NXR/NAR) is important for $^{18}\epsilon_{app}$ but not for $^{15}\epsilon_{app}$ (red curves, Figures 5A, B). Following the reasoning based on diffusive gradients, the increase in $^{18}\epsilon_{app}$ with NXR can be explained by preferential production of $N^{18}O_3^-$ in the oxidized surface layers. This is conceivable because the $\delta^{18}O$ of newly nitrified NO_3^- is determined by the $\delta^{18}O$ of O_2 and H_2O and the inverse O isotope effect of NXR (ϵ_{NXR} = -7 ‰). Since newly produced NO_2^- has a $\delta^{18}O$ of -2.3 ‰ and is oxidized with an inverse isotope effect, the $\delta^{18}O$ of newly nitrified NO_3^- will always be higher than the $\delta^{18}O$ of NO_3^- reduced (ϵ_{NAR} = 9 ‰). $^{18}\epsilon_{app}$ rises sharply to 1.8 ‰ for NXR/NAR = 20%. (Higher ratios could not be simulated in the model due to diffusive constraints on the O_2 flux). This trend is carried through to the $^{18}\epsilon_{app}$:$^{15}\epsilon_{app}$ trajectory that also shows a steep increase (red curve, Figure 5C). NXR, therefore, is also a viable candidate for producing $^{18}\epsilon_{app}$:$^{15}\epsilon_{app}$ > 1 in benthic chambers, as proposed for the water column (Granger and Wankel, 2016).

The model results show that $^{15}\epsilon_{Sed}$ is more sensitive to AMO and AMX compared to NXR, largely due to escape of residual $^{15}NH_4^+$ from the sediment (Lehmann et al., 2007; Alkhatib et al., 2012). Although anammox also has a large N isotope effect of 24 ‰ for NH_4^+ oxidation, it does not present as similarly strong of a dynamic as AMO. Reasons for this are difficult to disentangle due to the tight coupling of the N turnover pathways, but the depth in the sediment where AMO and AMX take place may be important. Ammonium oxidation is restricted to the oxidized surface sediment that is only a few millimeters thick, which allows residual $^{15}NH_4^+$ to quickly escape to the bottom water. Anammox, in contrast, occurs over a greater depth interval where NO_3^- and NO_2^- are available (Dalsgaard et al., 2005), implying a greater path length for residual $^{15}NH_4^+$ to diffuse into the bottom water. We suggest that this raises the likelihood that residual $^{15}NH_4^+$ can be oxidized by AMO or AMX, thereby muting the intrinsic isotope fingerprint of AMX on $^{15}\epsilon_{Sed}$. High rates of AMX (and AMO) even tend to decrease $^{15}\epsilon_{Sed}$, presumably because the total flux of NH_4^+ leaving the sediment is reduced at higher consumption rates.

A final point of significance is that $^{15}\epsilon_{Sed}$ and $^{15}\epsilon_{app}$ display opposing trends with regards to AMO. At low rates, AMO is associated with a decrease in $^{15}\epsilon_{app}$, whilst simultaneously increasing $^{15}\epsilon_{Sed}$, and vice-versa at high rates (blue curves Figures 5A, D). $^{15}\epsilon_{app}$ is not, therefore, a reliable indicator of the total sediment N isotope effect, $^{15}\epsilon_{Sed}$. The interplay of the N

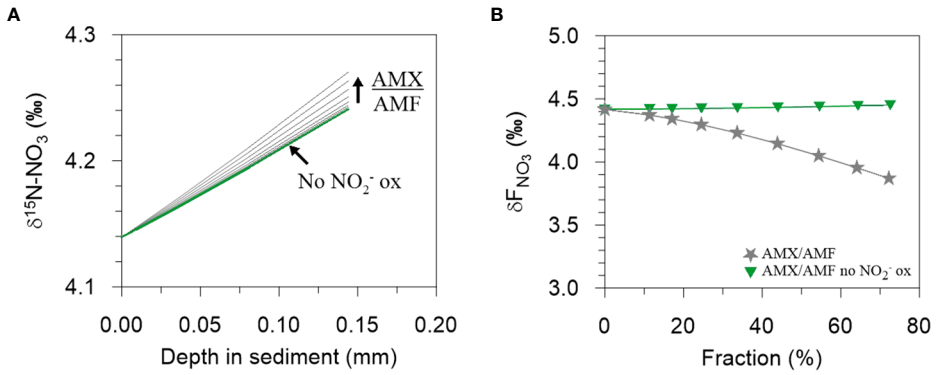

FIGURE 6
The effect on increasing AMX/AMF on **(A)** the δ^{15}N-NO_3 of porewater NO_3^- at the sediment surface and on **(B)** the δ^{15}N of the NO_3^- flux into the sediment. In **(A)**, an increase in AMX/AMF leads to a steepening of the δ^{15}N-NO_3 gradient and consequently, in **(B)**, to a decrease in $\delta_{F_{NO3}}$. Each curve in **(A)** has a corresponding symbol in **(B)**. The green lines in **(A)** are almost superimposed, reflecting a negligible change in δ^{15}N-NO_3 when NO_2^- oxidation by AMX is turned off. See Figure 5 for more details.

cycle leads to a difference between $^{15}\epsilon_{Sed}$ and $^{15}\epsilon_{app}$ that can be several ‰ at intermediate AMO/AMF values. This is a non-trivial amount considering that the oceanic N isotope balance is sensitive to small changes in the benthic N isotope effect (Brandes and Devol, 2002). For the continental margin, where most benthic denitrification takes place, the contribution of the NH_4^+ flux to the total benthic N isotope effect may be as important as NO_3^-. Consequently, δ^{15}N-NH_4 measurements in benthic chambers should be prioritized alongside δ^{15}N-NO_3.

5.3 Interannual variability of nutrient fluxes

As with most continental margins, benthic fluxes and N turnover pathways on the Mauritanian margin at 18°N reveal an intensification of nutrient recycling on the shelf and a sharp decrease offshore (Jahnke et al., 1990). This trend is driven by the increasingly recalcitrant nature of bulk sedimentary POC and POC rain rate with water depth (Dale et al., 2014).

The deposition flux of labile POC to the seafloor is positively correlated with benthic denitrification, and high rates of fixed N loss to N_2 are observed in both fine-grained and sandy continental shelves (Middelburg et al., 1996; Cook et al., 2006). The mean fraction of POC respired by denitrification on the Mauritanian margin (24%, Figure 1C) is higher than the global average of ≤10% (Middelburg et al., 1996). This can be explained by the amplification of denitrification in sediments underlying oxygen – deficient bottom waters due to less inhibition by O_2. The impact of denitrification is to raise the RQ since it produces DIC whilst not impacting TOU. If the 24% of POC that is remineralized by denitrification on the margin would instead be channeled through aerobic pathways, we might expect the TOU to increase by a similar amount with a corresponding decrease in RQ from 1.5 to 1.2. This is higher than the theorical value of 0.7 based on complete aerobic mineralization of organic matter with an average phytoplankton composition (Anderson, 1995) and supports the idea that benthic carbonate dissolution is driving an excess DIC flux across the margin.

The loss of fixed N relative to PO_4^{3-} generates N-depleted recycling fluxes (negative N*) compared to the standard phytoplankton N:P composition of ~16. If the calculated denitrification rates are added to F_{N^*}, the mean F_{N^*} increases from -2.8 to -1 mmol m^{-2} d^{-1}. indicating that N loss accounts for roughly two thirds of the negative N* flux. Enhanced PO_4^{3-} release under low-oxygen bottom waters probably accounts for the remaining third (Schroller-Lomnitz et al., 2019). Low or negative N* fluxes are characteristic of sediments under oxygen-deficient waters. Outside of these areas, where O_2 levels are > 100 µM, N-depleted fluxes are much more muted (Bohlen et al., 2012), partly due to more efficient sequestration of PO_4^{3-} by adsorption onto iron (oxyhydr)oxide minerals (Sundby et al., 1986). Mixing of low N:P waters from the benthic boundary layer into oxygen-poor water columns has the potential to enhance N_2 fixation, leading to a positive feedback between primary production, O_2 drawdown and benthic P release (Kemena et al., 2019).

On average, NH_4^+ and PO_4^{3-} fluxes on the shelf were 2 to 3 times higher in June 2014 compared to 2011 (Dale et al., 2014; Schroller-Lomnitz et al., 2019). NO_3^- and H_4SiO_4 fluxes were also elevated by 40 and 25%, respectively. Mean TOU in 2011 and 2014 was the same (ca. 10 mmol m^{-2} d^{-1}), and benthic carbon respiration rates on the shelf in 2014 were similar ($RPOC_{TOT}$ = 10 – 11 mmol m^{-2} d^{-1}). Given that the release of NH_4^+ and PO_4^{3-} from sediments is typically regulated by nitrification and adsorption by iron (oxyhydr)oxide minerals,

respectively (Sundby et al., 1986; Sloth et al., 1992), the higher NH_4^+ and PO_4^{3-} fluxes in 2014 suggest that the bottom waters might have become more reducing since 2011. Indeed, a long-term decline of O_2 concentrations in the ETNA has received much publicity (Stramma et al., 2008; Schmidtko et al., 2017). Our data corroborate these findings, with a decrease in minimum bottom water O_2 concentrations on the shelf from 42 µM in 2011 (Dale et al., 2014) to 25 µM in 2014 (Table 1).

One could conclude that the observed increase in NH_4^+ and PO_4^{3-} fluxes between 2011 and 2014 is caused by the long-term decrease in bottom water O_2. Yet, other contributing factors that are not easily quantifiable deserve careful consideration, such as (i) seasonal accumulation and depletion of nutrients in porewaters (e.g. Dale et al., 2013), (ii) changes in the faunal community structure and sediment reworking rates (Dale et al., 2013; Gier et al., 2017), (iii) low frequency changes in O_2 respiration close to the seabed associated with particle resuspension (Thomsen et al., 2019), and (iv) the episodic formation and export of oxygen-poor mesoscale eddies over the shelf on quasi-monthly time-scales (Thomsen et al., 2019). The magnitude of the O_2 decrease between 2011 and 2014 observed on the landers (17 µM) is also much higher than observed deoxygenation rates in the ETNA of ca. 0.5 µmol kg^{-1} yr^{-1} (Stramma et al., 2008). Long-term monitoring of sediment fluxes is needed to address this issue more precisely, preferably using autonomous methodologies such as bottom crawlers that can operate independently of costly ship-based surveys (Wenzhöfer et al., 2016). Until the technology to do so becomes more accessible, future projections of the nutrient budgets and the economic sustainability of fisheries in tropical upwelling regions will carry larger uncertainties (Wallmann et al., 2022).

6 Conclusions

This study presents *in situ* fluxes of O_2, DIC, nutrients and stable isotopes of dissolved inorganic nitrogen species in benthic chambers deployed on the Mauritanian margin in 2014. The aim was to quantify the recycling rates of biogenic debris with particular emphasis on the N cycle. The trends in benthic fluxes were generally similar to those measured in an earlier campaign to the region in 2011, and associated with a decrease in organic matter remineralization and denitrification rates with water depth. Notably, though, the fluxes of NH_4^+ and PO_4^{3-} on the shelf were 2 – 3 times higher in 2014. We were unable to pinpoint the cause of this increase from only two sets of field data. Long-term, or more frequent, monitoring of sediment-water interactions is needed to determine whether the seafloor is becoming more reducing and to elucidate possible linkages with the observed long-term decline in O_2 concentration in the tropical Atlantic. Elevated release of PO_4^{3-} from the standing stock of iron-bound P might stimulate the productivity of surface waters and continue to drive down subsurface O_2 levels, leading to a positive feedback between benthic PO_4^{3-} release and deoxygenation.

The mean isotopic fractionations of N ($^{15}\epsilon_{app}$) and O ($^{18}\epsilon_{app}$) accompanying benthic NO_3^- uptake were low and in good agreement with previously reported isotope effects for NO_3^- respiration in marine sediments. Analysis of the data using a numerical model showed that the overall benthic N isotope effect ($^{15}\epsilon_{sed}$) that includes the efflux of ^{15}N-enriched NH_4^+ from the seafloor, and the one that is of relevance to the global N isotope budget, bears no straightforward relationship with $^{15}\epsilon_{app}$. The model predicted $^{15}\epsilon_{Sed}$ = 3.6 ‰ for the Mauritanian shelf which, whilst lower than observed isotope effects of pelagic N loss in oxygen-deficient regions, adds to the growing body of evidence that the assumption of a universally low or negligible benthic N isotope effect is not applicable to oxygen-deficient settings.

The isotope model was used to constrain the relative rates of N turnover processes in the sediment. The model showed that observed trajectories in $^{18}\epsilon_{app}$:$^{15}\epsilon_{app}$ > 1 on the shelf were likely the result of aerobic ammonium oxidation and nitrite oxidation in surface sediments. Anammox has little influence on $^{18}\epsilon_{app}$:$^{15}\epsilon_{app}$ in this setting. This finding may be more widely applicable because the isotopic impact of anammox is less easily communicated to the water column than ammonium and nitrite oxidation. Anammox, however, tends to increase $^{15}\epsilon_{sed}$ if the fraction of NH_4^+ consumed is not too high. Our model suggests that NO_2^- isotope data from benthic chambers would help to constrain further the rates of N turnover in sediments, provided that the analytical challenge of low sample volumes from benthic chambers and low NO_2^- concentrations can be overcome.

Data availability statement

The datasets presented in this study can be found in online repositories. The names of the repository/repositories and accession number(s) can be found below: https://doi.pangaea.de/10.1594/PANGAEA.928206 https://doi.pangaea.de/10.1594/PANGAEA.941569.

Author contributions

AD conceived and wrote the paper. AD, DC, US-L and SS conducted fieldwork and chemical analyses. KD and FK performed isotope measurements. All authors contributed to the article and approved the submitted version.

Funding

This work is supported by the Sonderforschungsbereich 754 “Climate – Biogeochemistry Interactions in the Tropical Ocean”

(www.sfb754.de) financed by the Deutsche Forschungsgemeinschaft (DFG), and also by the German Federal Ministry of Education and Research (BMBF, funding ref. no. 03F0815A) through the research project REEBUS (Role of Eddies in the Carbon Pump of Eastern Boundary Upwelling Systems).

Acknowledgments

We thank A. Petersen, M. Türk, and S. Cherednichenko for their assistance in deploying the landers, and B. Domeyer, V. Thönissen, S. Trinkler, S. Kriwanek, A. Bleyer, R. Suhrberg, F. Jung geochemical analyses. We also thank Thomas Hansen (GEOMAR) for measuring the C and N isotopes in sediment samples and to Fabian Jung for assisting with the BIGO isotope measurements. We are grateful to the crew of RV Meteor and RV Maria S. Merian for their enthusiastic support. We express our gratitude to Annie Bourbonnais for editorial handling of the manuscript, and to the reviewers for their expertise and input that improved the finalized version.

Conflict of interest

The authors declare that the research was conducted in the absence of any commercial or financial relationships that could be construed as a potential conflict of interest.

Publisher's note

Supplementary material

The Supplementary Material for this article can be found online at: https://www.frontiersin.org/articles/10.3389/fmars.2022.902062/full#supplementary-material

References

Alkhatib, M., Lehmann, M. F., and del Giorgio, P. A. (2012). The nitrogen isotope effect of benthic remineralization–nitrification–denitrification coupling in an estuarine environment. *Biogeosciences* 9, 1633–1646. doi: 10.5194/bg-9-1633-2012

Altabet, M. A. (2007). Constraints on oceanic n balance/imbalance from sedimentary. *Biogeosciences* 4, 75–86. doi: 10.5194/bg-4-75-2007

Anderson, L. A. (1995). On the hydrogen and oxygen content of marine phytoplankton. *Deep-Sea Res. Part I-Oceanogr. Res. Pap.* 42, 1675–1680. doi: 10.1016/0967-0637(95)00072-E

Bender, M. L. (1990). The $\delta^{18}O$ of dissolved O_2 in seawater: A unique tracer of circulation and respiration in the deep sea. *J. Geophys. Res.* 95, 22243–22252. doi: 10.1029/JC095iC12p22243

Berner, R. A. (1980). *Early diagenesis–a theoretical approach. Princeton univ* (Princeton, N. J: Press).

Bohlen, L., Dale, A. W., Sommer, S., Mosch, T., Hensen, C., Noffke, A., et al. (2011). Benthic nitrogen cycling traversing the Peruvian oxygen minimum zone. *Geochim. Cosmochim. Acta* 75, 6094–6111. doi: 10.1016/j.gca.2011.08.010

Bohlen, L., Dale, A. W., and Wallmann, K. (2012). Simple transfer functions for calculating benthic fixed nitrogen losses and C:N:P regeneration ratios in global biogeochemical models. *Glob. Biogeochem. Cy.* 26, GB3029. doi: 10.1029/2011GB004198

Böhlke, J. K., Mroczkowski, S. J., and Coplen, T. B. (2003). Oxygen iso-topes in nitrate: new reference materials for18O :17O :16O mea-surements and observations on nitrate-water equilibration. *Rapid Commun. Mass Spectrom.* 17, 1835–1846. doi: 10.1002/rcm.1123

Bourbonnais, A., Altabet, M. A., Charoenpong, C. N., Larkum, J., Hu, H., Bange, H. W., et al. (2015). N-loss isotope effects in the Peru oxygen minimum zone studied using a mesoscale eddy as a natural tracer experiment. *Global Biogeochem. Cycles* 29, 793–811. doi: 10.1002/2014GB005001

Brandes, J. A., and Devol, A. H. (1997). Isotopic fractionation of oxygen and nitrogen in coastal marine sediments. *Geochim. Cosmochim. Acta* 61, 1793–1801. doi: 10.1016/S0016-7037(97)00041-0

Brandes, J. A., and Devol, A. H. (2002). A global marine-fixed nitrogen isotopic budget: Implications for Holocene nitrogen cycling *Global Biogeochem. Cycles* 16 (4), 1120. doi: 10.1029/2001GB001856

Brüchert, V., Jørgensen, B. B., Neumann, K., Riechmann, D., Schlösser, M., and Schulz, H. (2003). Regulation of bacterial sulfate reduction and hydrogen sulfide fluxes in the central namibian coastal upwelling zone. *Geochim. Cosmochim. Acta* 67, 4505–4518. doi: 10.1016/S0016-7037(03)00275-8

Brunner, B., Contreras, S., Lehmann, M. F., Matantseva, O., Rollog, M., Kalvelage, T., et al. (2013). Nitrogen isotope effects induced by anammox bacteria. *Proc. Natl. Acad. Sci. U.S.A.* 110, 18994–18999. doi: 10.1073/pnas.1310488110

Brzezinski, M. A. (1985). The Si:C:N ratio of marine diatoms: Interspecific variability and the effect of some environmental variables. *J. Phycol.* 21, 347–357. doi: 10.1111/j.0022-3646.1985.00347.x

Buchwald, C., and Casciotti, K. L. (2010). Oxygen isotopic fractionation and exchange during bacterial nitrite oxidation. *Limnol. Oceanogr.* 55, 1064–1074. doi: 10.4319/lo.2010.55.3.1064

Buchwald, C., and Casciotti, K. L. (2013). Isotopic ratios of nitrite as tracers of the sources and age of oceanic nitrite. *Nat. Geosci.* 6, 1–6. doi: 10.1038/ngeo1745

Buchwald, C., Homola, K., Spivack, A. J., Estes, E. R., Murray, R. W., and Wankel, S. D. (2018). Isotopic constraints on nitrogen transformation rates in the deep sedimentary marine biosphere. *Glob. Biogeochem. Cy.* 32, 1688–1702. doi: 10.1029/2018GB005948

Buchwald, C., Santoro, A. E., McIlvin, M. R., and Casciotti, K. L. (2012). Oxygen isotopic composition of nitrate and nitrite produced by nitrifying cocultures and natural marine assemblages. *Limnology Oceanography* 57, 1361–1375. doi: 10.4319/lo.2012.57.5.1361

Burdige, D. J. (2006). *Geochemistry of marine sediments* (Princeton: Princeton University Press), 609.

Carr, M.-E. (2001). Estimation of potential productivity in Eastern boundary currents using remote sensing. *Deep-Sea Res. Part II Top. Stud. Oceanogr.* 49, 59–80. doi: 10.1016/S0967-0645(01)00094-7

Casciotti, K. L. (2009). Inverse kinetic isotope fractionation during bacterial nitrite oxidation. *Geochim. Cosmochim. Acta* 73, 2061–2076. doi: 10.1016/j.gca.2008.12.022

Casciotti, K. L. (2016). Nitrite isotopes as tracers of marine n cycle processes. *Philos. Trans. R. Soc A* 374, 20150295. doi: 10.1098/rsta.2015.0295

Casciotti, K. L., Buchwald, C., and McIlvin, M. (2013). Implications of nitrate and nitrite isotopic measurements for the mechanisms of nitrogen cycling in the Peru oxygen deficient zone. *Deep-Sea Res. I* 80, 78–93. doi: 10.1016/j.dsr.2013.05.017

Casciotti, K. L., and McIlvin, M. R. (2007). Isotopic analyses of nitrate and nitrite from reference mixtures and application to Eastern tropical north pacific waters. *Mar. Chem.* 107, 184–201. doi: 10.1016/j.marchem.2007.06.021

Casciotti, K. L., McIlvin, M. R., and Buchwald, C. (2010). Oxygen isotopic exchange and fractionation during bacterial ammonia oxidation. *Limnol. Oceanogr.* 55, 753–762. doi: 10.4319/lo.2010.55.2.0753

Casciotti, K. L., Sigman, D. M., Galanter Hastings, M., and Böhlke, J. K. (2002). Measurement of the oxygen isotopic composition of nitrate in seawater and freshwater using the denitrifier method. *Analyt. Chem.* 74, 4905–4912. doi: 10.1021/ac020113w

Casciotti, K. L., Sigman, D. M., and Ward, B. B. (2003). Linking diversity and stable isotope fractionation in ammonia-oxidizing bacteria. *Geomicrobiol. J.* 20, 335–353. doi: 10.1080/01490450303895

Cook, P. L. M., Wenzhoefer, F., Rysgaard, S., Galaktionov, O. S., Meysman, F. J. R., Eyre, B. D., et al. (2006). Quantification of denitrification in permeable sediments: Insights from a two–dimensional simulation analysis and experimental data. *Limnol. Oceanogr. Meth.* 4, 294–307. doi: 10.4319/lom.2006.4.294

Cowie, G., Mowbray, S., Kurian, S., Sarkar, A., White, C., Anderson, A., et al. (2014). Comparative organic geochemistry of Indian margin (Arabian Sea) sediments: estuary to continental slope. *Biogeosciences* 11, 6683–6696. doi: 10.5194/bg-11-6683-2014

Dähnke, K., and Thamdrup, B. (2013). Nitrogen isotope dynamics and fractionation during sedimentary denitrification in boknis eck, Baltic Sea. *Biogeosciences* 10, 3079–3088. doi: 10.5194/bg-10-3079-2013

Dale, A. W., Bertics, V. J., Treude, T., Sommer, S., and Wallmann, K. (2013). Modeling benthic-pelagic nutrient exchange processes and porewater distributions in a seasonally-hypoxic sediment: evidence for massive phosphate release by *Beggiatoa*? *Biogeosciences* 10, 629–651. doi: 10.5194/bg-10-629-2013

Dale, A. W., Bourbonnais, A., Altabet, M., Wallmann, K., and Sommer, S. (2019). Isotopic fingerprints of benthic nitrogen cycling in the Peruvian oxygen minimum zone. *Geochim. Cosmochim. Acta* 245, 406–425. doi: 10.1016/j.gca.2018.10.025

Dale, A. W., Sommer, S., Lomnitz, U., Montes, I., Treude, T., Liebetrau, V., et al. (2015). Organic carbon production, mineralisation and preservation on the Peruvian margin. *Biogeosciences* 12, 1537–1559. doi: 10.5194/bg-12-1537-2015

Dale, A. W., Sommer, S., Ryabenko, E., Noffke, A., Bohlen, L., Wallmann, K., et al. (2014). Benthic nitrogen fluxes and fractionation of nitrate in the Mauritanian oxygen minimum zone (Eastern tropical north Atlantic). *Geochim. Cosmochim. Acta* 134, 234–256. doi: 10.1016/j.gca.2014.02.026

Dalsgaard, T., Thamdrup, B., and Canfield, D. E. (2005). Anaerobic ammonium oxidation (anammox) in the marine environment. *Res. Microbiol.* 156, 457–464. doi: 10.1016/j.resmic.2005.01.011

Deutsch, C., Sigman, D. M., Thunell, R. C., MEckler, A. N., and Haug, G. H. (2004). Isotopic constraints on glacial/interglacial changes in the oceanic nitrogen budget. *Glob. Biogeochem. Cy.* 18, GB4012. doi: 10.1029/2003GB002189

Devol, A. H., Uhlenhopp, A. G., Naqvi, S. W. A., Brandes, J. A., Jayakumar, D. A., Naik, H., et al. (2006). Denitrification rates and excess nitrogen gas concentrations in the Arabian Sea oxygen deficient zone. *Deep. Res. I* 53, 1533–1547. doi: 10.1016/j.dsr.2006.07.005

Fischer, G., Neuer, S., Davenport, R., Romero, O., Ratmeyer, V., Donner, B., et al. (2010). "The Northwest African margin, in: Carbon and nutrient fluxes in continental margins," in *A global synthesis*. Eds. K.-K. Liu, L. Atkinson, R. Quiñones and L. Talaue-McManus (Berlin: IGBP Book Series, Springer), 77–103.

Fütterer, D. K. (1983). "The modern upwelling record off northwest Africa, in coastal upwelling: Its sedimentary record, part b," in *Sedimentary records of ancient coastal upwelling*. Eds. J. Thiede and E. Suess (Plenum, New York: Springer), 105–121.

Gaye, B., Nagel, B., Dähnke, K., Rixen, T., and Emeis, K.-C. (2013). Evidence of parallel denitrification and nitrite oxidation in the ODZ of the Arabian Sea from paired stable isotopes of nitrate and nitrite. *Glob. Biogeochem. Cy.* 27, 1059–1071. doi: 10.1002/2011GB004115

Gier, J., Löscher, C. R., Dale, A. W., Sommer, S., Lomnitz, U., and Treude, T. (2017). Benthic dinitrogen fixation traversing the oxygen minimum zone off Mauritania (NW Africa). *Front. Mar. Sci.* 4. doi: 10.3389/fmars.2017.00390

Granger, J., Prokopenko, M. G., Sigman, D. M., Mordy, C. W., Morse, Z. M., Morales, L. V., et al. (2011). Coupled nitrification-denitrification in sediment of the eastern Bering Sea shelf leads to ^{15}N enrichment of fixed n in shelf waters. *J. Geophys. Res.* 116. doi: 10.1029/2010JC006751

Granger, J., Sigman, D. M., Lehmann, M. F., and Tortell, P. D. (2008). Nitrogen and oxygen isotope fractionation during dissimilatory nitrate reduction by denitrifying bacteria. *Limnol. Oceanogr.* 53, 2533–2545. doi: 10.4319/lo.2008.53.6.2533

Granger, J., and Wankel, S. D. (2016). Environmental overprinting of nitrate isotopes. *Proc. Nat. Acad. Sci.* 113 (42), E6391–E6400. doi: 10.1073/pnas.1601383113

Gruber, N. (2008). The marine nitrogen cycle and atmospheric CO_2.In: *Nitrogen in the Marine Environment* (*Second* Edition) DG Capone, DA Bronk, MR Mulholland and EJ Carpenter (Academic Press) 1–50. doi: 10.1016/B978-0-12-372522-6.00001-3

Gruber, N., and Sarmiento, J. (1997). Global patterns of marine nitrogen fixation and denitrification. *Glob. Biogeochem. Cy.* 11, 235–266. doi: 10.1029/97GB00077

Hansen, T., and Sommer, U. (2007). Increasing the sensitivity of $\delta^{13}C$ and $\delta^{15}N$ abundance measurements by a high sensitivity elemental analyser connected to an isotope ratio mass spectrometer. *Rapid Commun. Mass Spectrom.* 21, 314–318. doi: 10.1002/rcm.2847

Hartmann, M., Müller, P. J., Suess, E., and van der Weijden, C. H. (1976). Chemistry of late quaternary sediments and their interstitial waters from the NW African continental margin. *Meteor Forschungsergebnisse. Reihe C: Geologie und Geophysik* 24, 1–67.

Huntsman, S. A., and Barber, R. T. (1977). Primary production off northwest Africa: the relationship to wind and nutrient conditions. *Deep Sea Res.* 24, 25–33. doi: 10.1016/0146-6291(77)90538-0

Jahnke, R. A., and Jahnke, D. B. (2004). Calcium carbonate dissolution in deep sea sediments: Reconciling microelectrode, pore water and benthic flux chamber results. *Geochim. Cosmochim. Acta* 68, 47–59. doi: 10.1016/S0016-7037(03)00260-6

Jahnke, R. A., Reimers, C. E., and Craven, D. B. (1990). Organic matter recycling at the seafloor: intensification near ocean margins. *Nature* 348, 50–54. doi: 10.1038/348050a0

Jourabchi, P., Van Cappellen, P., and Reginer, P. (2005). Quantitative interpretation of pH distributions in aquatic sediments: A reaction-transport modeling approach. *Am. J. Sci.* 305, 919–956. doi: 10.2475/ajs.305.9.919

Jorgensen, B. B., Wenzh.fer, F., Egger, M, and Glud, R. N. (2022). Sediment oxygen consumption: Role in the global marine carbon cycle. *Earth-Science Reviews* 228, 103987. doi: 10.1016/j.earscirev.2022.103987

Karstensen, J., Stramma, L., and Visbeck, M. (2008). Oxygen minimum zones in the eastern tropical Atlantic and pacific oceans. *Prog. Oceanogr.* 77, 331–350. doi: 10.1016/j.pocean.2007.05.009

Kemena, T. P., Landolfi, A., Oschlies, A., Wallmann, K., and Dale, A. W. (2019). Ocean phosphorus inventory: large uncertainties in future projections on millennial timescales and their consequences for ocean deoxygenation. *Earth Syst. Dynam.* 10, 539–553. doi: 10.5194/esd-10-539-2019

Klenz, T., Dengler, M., and Brandt, P. (2018). Seasonal variability of the Mauritania current and hydrography at 18°N. *J. Geophys. Res. Oceans* 123, 8122–8137. doi: 10.1029/2018JC014264

Krahmann, G., Arévalo-Martínez, D. L., Dale, A. W., Dengler, M., Engel, A., Glock, N., et al. (2021). Climate-biogeochemistry interactions in the tropical ocean: data collection and legacy. *Front. Mar. Sci.* 8. doi: 10.3389/fmars.2021.723304

Kritee, K., Sigman, D. M., Granger, J., Ward, B. B., Jayakumar, A., and Deutsch, C. (2012). Reduced isotope fractionation by denitrification under conditions relevant to the ocean. *Geochim. Cosmochim. Acta* 92, 243–259. doi: 10.1016/j.gca.2012.05.020

Lam, P., and Kuypers, M. M. M. (2011). Microbial nitrogen cycling processes in oxygen minimum zones. *Ann. Rev. Mar. Sci.* 3, 317–345. doi: 10.1146/annurev-marine-120709-142814

Lehmann, M. F., Sigman, D. M., and Berelson, W. M. (2004). Coupling the $^{15}N/^{14}N$ and $^{18}O/^{16}O$ of nitrate as a constraint on benthic nitrogen cycling. *Mar. Chem.* 88, 1–20. doi: 10.1016/j.marchem.2004.02.001

Lehmann, M. F., Sigman, D. M., McCorkle, D. C., Granger, J., Hoffmann, S., Cane, G., et al. (2007). The distribution of nitrate $^{15}N/^{14}N$ in marine sediments and the impact of benthic nitrogen loss on the isotopic composition of oceanic nitrate. *Geochim. Cosmochim. Acta* 71, 5384–5404. doi: 10.1016/j.gca.2007.07.025

Marioitti, A., Germon, J. C., Hubert, P., Kaiser, P., Letolle, R., Tardieux, A., et al. (1981). Experimental determination of nitrogen kinetic isotope fractionation: Some principles; illustration for the denitrification and nitrification processes. *Plant Soil* 62, 413–430. doi: 10.1007/BF02374138

Mcilvin, M. R., and Altabet, M. A. (2005). Chemical conversion of nitrate and nitrite to nitrous oxide for nitrogen and oxygen isotopic analysis in freshwater and seawater. *Anal. Chem.* 77, 5589–5595. doi: 10.1021/ac050528s

Meyers, P. A. (1994). Preservation of elemental and isotopic source identification of sedimentary organic matter. *Chem. Geol.* 114, 289–302. doi: 10.1016/0009-2541(94)90059-0

Middelburg, J. J. (1989). A simple rate model for organic matter decomposition in marine sediments. *Geochim. Cosmochim. Acta* 53, 1577–1581. doi: 10.1016/0016-7037(89)90239-1

Middelburg, J. J., Soetaert, K., Herman, P. M. J., and Heip, C. H. R. (1996). Denitrification in marine sediments: A model study. *Glob. Biogeochem. Cy.* 10, 661–673. doi: 10.1029/96GB02562

Mittelstaedt, E. (1983). The upwelling area off Northwest Africa – a description of phenomena related to coastal upwelling. *Prog. Oceanogr.* 12, 307–331. doi: 10.1016/0079-6611(83)90012-5

Möbius, J. (2013). Isotope fractionation during nitrogen remineralization (ammonification): Implications for nitrogen isotope biogeochemistry. *Geochim. Cosmochim. Acta* 105, 422–432. doi: 10.1016/j.gca.2012.11.048

Mortazavi, B., and Chanton, J. P. (2004). Use of keeling plots to determine sources of dissolved organic carbon in nearshore and open ocean systems. *Limnol. Oceanogr.* 49, 102–110. doi: 10.4319/lo.2004.49.1.0102

Prokopenko, M. G., Hirst, M. B., De Brabandere, L., Lawrence, D. J. P., Berelson, W. M., Granger, J., et al. (2013). Nitrogen losses in anoxic marine sediments driven by *Thioploca*-anammox bacterial consortia. *Nature* 500, 194–198. doi: 10.1038/nature12365

Rooze, J., and Meile, C. (2016). The effect of redox conditions and bioirrigation on nitrogen isotope fractionation in marine sediments. *Geochim. Cosmochim. Acta* 184, 227–239. doi: 10.1016/j.gca.2016.04.040

Ryabenko, E., Altabet, M. A., and Wallace, D. W. R. (2009). Effect of chloride on the chemical conversion of nitrate to nitrous oxide for delta n–15 analysis. *Limnol. Oceanogr. Meth.* 7, 245–552. doi: 10.4319/lom.2009.7.545

Schafstall, J., Dengler, M., Brandt, P., and Bange, H. (2010). Tidal induced mixing and diapycnal nutrient fluxes in the Mauritanian upwelling region. *J. Geophys. Res.* 115, C10014. doi: 10.1029/2009JC005940

Schmidtko, S., Stramma, L., and Visbeck, M. (2017). Decline in global oceanic oxygen content during the past five decades. *Nature* 542, 335–339. doi: 10.1038/nature21399

Schroller-Lomnitz, U., Hensen, C., Dale, A. W., Scholz, F., Clemens, D., Sommer., S., et al. (2019). Dissolved benthic phosphate, iron and carbon fluxes in the Mauritanian upwelling system and implications for ongoing deoxygenation. *Deep-Sea Res. I* 143, 70–84. doi: 10.1016/j.dsr.2018.11.008

Sigman, D. M., Casciotti, K. L., Andreani, M., Barford, C., Galanter, M., and Böhlke, J. K. (2001). A bacterial method for the nitrogen isotopic analysis of nitrate in seawater and freshwater. *Anal. Chem.* 73, 4145–4153. doi: 10.1021/ac010088e

Sigman, D. M., DiFiore, P. J., Hain, M. P., Deutsch, C., Wang, Y., Karl, D. M., et al. (2009). The dual isotopes of deep nitrate as a constraint on the cycle and budget of oceanic fixed nitrogen. *Deep-Sea Res. I Oceanogr. Res. Pap.* 56, 1419–1439. doi: 10.1016/j.dsr.2009.04.007

Sigman, D. M., Granger, J., DiFiore, P. J., Lehmann, M. F., Ho, R., Cane, G., et al. (2006). Coupled nitrogen and oxygen isotope measurements of nitrate along the eastern north pacific margin. *Global Biogeochem. Cycles* 19, GB4022. doi: 10.1029/2005GB002458

Sloth, N. P., Nielsen, L. P., and Blackburn, T. H. (1992). Nitrification in sediment cores measured with acetylene inhibition. *Limnol. Oceanogr.* 37, 1108–1112. doi: 10.4319/lo.1992.37.5.1108

Sokoll, S., Lavik, G., Sommer, S., Goldhammer, T., Kuypers, M. M. M., and Holtappels, M. (2016). Extensive nitrogen loss from permeable sediments off north-West Africa. *J. Geophys. Res. Biogeosci.* 121, 1144–1157. doi: 10.1002/2015JG003298

Somes, C. J., Oschlies, A., and Schmittner, A. (2013). Isotopic constraints on the pre-industrial oceanic nitrogen budget. *Biogeosciences* 10, 5889–5910. doi: 10.5194/bg-10-5889-2013

Sommer, S., Adam, N., Becker, K., Dale, A. W., Hahn, J., Kampmeier, M., et al. (2020). *Role of eddies in the carbon pump of Eastern boundary upwelling systems, REEBUS, cruise no. M156, 03.07. – 01.08.2019 mindelo (Cap Verde) – mindelo* (Bonn: Meteor Berichte, M156. Gutachterpanel Forschungsschiffe), 53 pp. doi: 10.2312/cr_m156

Sommer, S., Dengler, M., and Treude, T. (2015). *Benthic element cycling, fluxes and transport of solutes across the benthic boundary layer in the Mauritanian oxygen minimum zone, (SFB754) - cruise no. M107, may 30 - July 03, 2014, fortaleza (Brazil) - las palmas (Spain). METEOR-berichte, M107* (Bremen: DFG-Senatskommission für Ozeanographie), 67 pp. doi: 10.2312/cr_m107

Sommer, S., Türk, M., Kriwanek, S., and Pfannkuche, O. (2008). Gas exchange system for extended *in situ* benthic chamber flux measurements under controlled oxygen conditions: First application – Sea bed methane emission measurements at captain arutyunov mud volcano. *Limnol. Oceanogr. Meth.* 6, 23–33. doi: 10.4319/lom.2008.6.23

Stolpovsky, K., Dale, A. W., and Wallmann, K. (2015). Toward a parameterization of global-scale organic carbon mineralization kinetics in surface marine sediments. *Glob. Biogeochem. Cy.* 29, 812–829. doi: 10.1002/2015GB005087

Stramma, L., Johnson, G. C., Sprintall, J., and Mohrholz, V. (2008). Expanding oxygen–minimum zones in the tropical oceans. *Science* 320, 655–658. doi: 10.1126/science.1153847

Strous, M., Fuerst, J. A., Kramer, E. H. M., Logemann, S., Muyzer, G., van de Pas-Schoonen, K. T., et al. (1999). Missing lithotroph identified as new planctomycete. *Nature* 400, 446–449. doi: 10.1038/22749

Sundby, B., Anderson, L. G., Hall, P. O. J., Iverfeldt, Å., van der Loeff, M. M. R., and Westerlund, S. F. G. (1986). The effect of oxygen on release and uptake of cobalt, manganese, iron and phosphate at the sediment-water interface. *Geochim. Cosmochim. Acta* 50 (6), 1281–1288. doi: 10.1016/0016-7037(86)90411-4

Thomsen, S., Karstensen, J., Kiko, R., Krahmann, G., Dengler, M., and Engel, A. (2019). Remote and local drivers of oxygen and nitrate variability in the shallow oxygen minimum zone off Mauritania in June 2014. *Biogeosciences* 16, 979–998. doi: 10.5194/bg-16-979-2019

Voss, M., Dippner, J. W., and Montoya, J. P. (2001). Nitrogen isotope patterns in the oxygen–deficient waters of the Eastern tropical north pacific ocean. *Deep–Sea Res. I* 48, 1905–1921. doi: 10.1016/S0967-0637(00)00110-2

Wallmann, K., José, Y. S., Hopwood, M. J., Somes, C. J., Dale, A. W., Scholz, F., et al. (2022). Biogeochemical feedbacks may amplify ongoing and future ocean deoxygenation: A case study from the Peruvian oxygen minimum zone. *Biogeochemistry* 159, 45–67. doi: 10.1007/s10533-022-00908-w

Wenzhöfer, F., Lemburg, J., Hofbauer, M., Lehmenhecker, S., and Färber, P. (2016). *TRAMPER – an autonomous crawler for long-term benthic oxygen flux studies in remote deep-sea ecosystems* (Monterey: OCEANS 2016 MTS/IEEE), 1–6.

Zhang, L., Altabet, M. A., Wu, T., and Hadas, O. (2007). Sensitive measurement of NH_4^+ $^{15}N/^{14}N$ (delta $^{15}NH_4^+$) at natural abundance levels in fresh and saltwaters. *Anal. Chem.* 79, 5297–5303. doi: 10.1021/ac070106d